Thermodynamic implications of confinement for a waterlike fluid

Thomas M. Truskett and Pablo G. Debenedetti[a)]
Department of Chemical Engineering, Princeton University, Princeton, New Jersey 08544

Salvatore Torquato
Department of Chemistry and Princeton Materials Institute, Princeton University, Princeton, New Jersey 08544

(Received 5 October 2000; accepted 6 November 2000)

A theoretical framework is introduced for studying the thermodynamics and phase behavior of a ''waterlike'' fluid film confined between hydrophobic plane surfaces. To describe the hydrogen-bonding interactions in the fluid film, an earlier analytical theory for uniform associating fluids is generalized. Two levels of approximation are presented. In the first, the reference fluid is assumed to be homogeneous. Here, the primary effect of the confining walls is to reduce the average number of favorable fluid–fluid interactions relative to the bulk fluid. The implications of this energetic penalty for the phase behavior and, in particular, the low-temperature waterlike anomalies of the fluid are examined. It is shown that the reduction of favorable fluid–fluid interactions can promote strong hydrophobic interactions between the confining surfaces at nanometer length scales, induced by the evaporation of the fluid film. In the second level of approximation, the inhomogeneous nature of the reference fluid is accounted for by a density functional theory. The primary effect of the density modulations is to promote or disrupt hydrogen bonding in distinct layers within the pore. Interestingly, when the reference fluid is treated as inhomogeneous, the theory predicts the possibility of a new low-temperature phase transition in the strongly confined fluid. © *2001 American Institute of Physics.* [DOI: 10.1063/1.1336569]

I. INTRODUCTION

Restricted geometries that contain thin films of water are common in engineering practice, geology, and biology. Examples include zeolites and clays,[1] minerals,[2] biological hydrogels,[3] vesicles,[4] mesoscopic surfactant assemblies,[5] ionic channels,[6] and even interstellar bodies.[7] Consequently, the modification of water's behavior due to interaction with a solid surface has great scientific and technological significance,[8–11] bearing relevance to corrosion inhibition, heterogeneous catalysis, the ascent of sap in plants, the stability and enzymatic activity of globular proteins, and the function of biological membranes. The recent drive to miniaturize and integrate chemical and physical processes for wet ''lab-on-a-chip'' technologies[12] further highlights the need to understand the effects of nanoscale confinement on water and aqueous solutions.

Although many valuable insights into the physics of confined phases have resulted from experiments, molecular simulations, and microscopic theories,[13–15] predicting the properties of even ''simple'' nonassociating fluids under confinement remains a daunting theoretical task. This is due, at least in part, to the sheer number of factors that can contribute to the modification of a fluid's bulk thermodynamic and transport properties, including: the size distribution, geometry, and connectivity of the confining pores in the *adsorbent*; the molecular size and architecture of the *adsorbate*; and the competition between adsorbate–adsorbate and adsorbate–adsorbent interactions. As a result of these additional considerations, materials in confined spaces can exhibit rich physical behaviors that are absent in the bulk.

From a thermodynamic perspective, the possibility arises for surface-driven phenomena (e.g., wetting, layering, and commensurate–incommensurate transitions) and pronounced shifts in the ''bulk'' phase transitions (i.e., vapor–liquid, vapor–solid, liquid–solid, and liquid–liquid).[13,15] Moreover, confinement can severely alter the dynamics of the liquid state. One intriguing example is the apparent formation of two distinct dynamical regions in confined fluids: an interfacial layer with decreased mobility close to the substrate and a ''core'' region farther from the substrate that exhibits faster relaxation processes.[16–20] As a result, the fluid in the interfacial layer vitrifies at a higher temperature than the fluid in the core.

The case of water under confinement is especially interesting, given that bulk water exhibits a number of unusual physical properties. The bulk liquid anomalies include negative thermal expansion coefficient ($\alpha_P<0$) over a broad range of temperature and pressure,[9,21–23] strongly increasing isobaric heat capacity (c_P) and isothermal compressibility (κ_T) upon isobaric cooling,[9,24–26] and increasing mobility upon isothermal compression.[9,27,28] Crystalline water is also complex,[29,30] exhibiting 13 distinct ice polymorphs in which each molecule is hydrogen-bonded to four neighbors in a nearly tetrahedral arrangement.

The anomalous properties of bulk water are enhanced at low temperature. In fact, below its glass transition temperature ($\approx$130 K at 1 bar), bulk glassy water (also called *amorphous ice*) is known to exhibit a phenomenon known as *polyamorphism*[31–33] in which two different forms, termed

a)Electronic mail: pdebene@princeton.edu

low-density amorphous ice (LDA) and high-density amorphous ice (HDA), are separated by a seemingly first-order transition. Evidence suggests that liquid water and its glassy phases are both thermodynamically and structurally continuous,[34–36] implying that the sharp changes in density that accompany the transformation from LDA into HDA are the structurally arrested manifestation of an underlying liquid–liquid transition. This interpretation is commonly referred to as the *two-critical-point* scenario because it attributes the anomalies of supercooled water to the presence of a second (metastable) critical point, where the first-order phase transition between LDA and HDA terminates. Although the two-critical-point scenario is not the only thermodynamically-consistent explanation for supercooled water's anomalies,[37–42] the experimentally measured melting curves of high-pressure forms of ice,[43,44] as well as the results from numerous computer simulations and theoretical calculations for model ''waterlike'' fluids,[42,45–49,43,50,51] suggest the possibility of a low-temperature liquid–liquid immiscibility.

Since bulk liquid water cannot be studied experimentally below its homogeneous nucleation temperature ($\approx$231 K at 1 bar), the hypothesis of a liquid–liquid transition has not been unambiguously verified. However, confinement may provide an alternative avenue for testing the two-critical-point hypothesis for water. In particular, recent neutron diffraction experiments on water confined in Vycor glass[52–54] and carbon powder,[55] as well as molecular dynamics simulations of confined waterlike fluids,[56,54,57] indicate that the presence of a solid interface severely distorts water's hydrogen-bond network, possibly inhibiting crystal nucleation. This conclusion is consistent with the fact that liquid water confined in vermiculite clays,[58,59] sequestered in polymer matrices,[35] and adsorbed on the surface of globular proteins[60] can be supercooled to temperatures far below its bulk freezing point. Thus, it is logical to suspect that confinement may permit the investigation of supercooled liquid water in the temperature range where the liquid–liquid phase transition is proposed to occur in the bulk. However, since the global phase behavior of water (including the location of the proposed liquid–liquid phase transition) will in turn be affected by confinement, it is important to develop theoretical tools that permit the investigation of the global phase behavior of water in restricted geometries.

As a first step in this direction, we present a simple theory for studying the thermodynamics and fluid-phase equilibria of an associating fluid film confined between two parallel hydrophobic substrates. The approach we use is based on a perturbation theory introduced by Schoen and Diestler[61] to study the thermodynamic behavior of a simple nonassociating fluid confined to a slit-pore. We extend their original approach to include fluid–fluid hydrogen-bonding interactions. The contribution to the free energy from the hydrogen bonds is determined from a generalization of a recently introduced analytical theory[42] that is able to reproduce bulk water's distinctive thermodynamic behavior (including anomalies in c_P, α_P, and κ_T, as well as the possibility of a polyamorphic phase transition). The thermodynamics and global phase behavior of the fluid film are then determined by solving the resulting perturbation theory using two different levels of approximation for the reference fluid. The first level is a mean-field theory that assumes the reference confined fluid to be homogeneous. In the second, more refined level of approximation, a density functional theory is used to account for the inhomogeneous nature of the reference fluid.

The theoretical investigation presented in this paper highlights two physically-intuitive confinement effects. The first can be summarized as follows: The introduction of two hydrophobic confining walls reduces the average number of favorable hydrogen-bonding interactions per molecule relative to the bulk fluid at the same density. This feature, which is captured by the theory at the mean-field level, causes the liquid–liquid critical point to shift to lower temperature, higher density, and higher pressure as the degree of confinement is increased. The reduction of favorable fluid–fluid interactions also promotes strong hydrophobic interactions between the confining walls at nanometer length scales,[62–67] induced by the evaporation of the intervening fluid film.

The second confinement effect is the introduction of density modulations into the fluid film. These modulations (accounted for in the second level of the theory) can promote or disrupt hydrogen bonding in distinct ''layers,'' modifying the dependence of the hydrogen-bonding energy on the average pore density. Interestingly, when the density modulations are incorporated into the perturbation theory, a third fluid–fluid transition emerges in the strongly confined fluid. The appearance of this third phase transition is discussed in terms of recent computer simulation results of water-like fluids confined between hydrophobic walls.[56,68]

For convenience, the predicted effects of confinement on the thermodynamics of the waterlike fluid film are summarized below.

Level 1 Theory: Homogeneous reference fluid:

(1) The liquid–vapor critical point shifts to lower temperature, lower pressure, and higher density relative to the bulk;
(2) The low-temperature liquid–liquid critical point shifts to lower temperature, higher pressure, and higher pore density relative to the bulk;
(3) For weakly attractive substrates, confinement-induced evaporation of the fluid film occurs at room temperature and nanoscale wall separations.

Level 2 Theory: Inhomogeneous reference fluid:

(1) The liquid–vapor critical point shifts to lower temperature, lower pressure, and higher density relative to the bulk;
(2) The low-temperature liquid–liquid critical point shifts to lower temperature and higher density relative to the bulk. The critical pressure exhibits a nonmonotonic dependence on pore width;
(3) A third fluid–fluid phase transition appears in the strongly confined film.

The paper is organized as follows. In Sec. II, we outline the continuum, thermodynamic description of a thin fluid

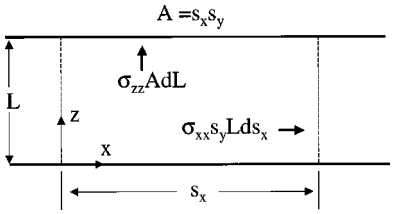

FIG. 1. Cross section of the finite ''lamella'' of fluid confined between rigid walls discussed in the text (adapted from Ref. 69). Note that the lower wall is stationary in the laboratory reference frame.

film confined between parallel substrates. The microscopic perturbation approach for an associating fluid film confined between hydrophobic planar substrates is given in Sec. III. In Sec. IV, the thermodynamics and global phase behavior of the film are presented for the two levels of approximation for the perturbation theory. Finally, in Sec. V, we present some concluding remarks.

II. THERMODYNAMICS OF THIN-FILM CONFINEMENT

To set the stage for presenting a microscopic theory for association in a slit-pore, it is useful to first develop the thermodynamics of thin-film confinement. In this section, we present a simple physical derivation of the fundamental relation governing changes in the internal energy of the fluid film U in terms of the natural independent variables (the entropy S, the pore width L, the fluid–solid interfacial area A at one of the confining walls, and the number of molecules N). Alternative thermodynamic potentials can then be obtained from the fundamental relationship through Legendre transforms. For a more comprehensive discussion of the thermodynamics of confined thin films, the reader is referred to the work of Diestler and Schoen.[69]

In what follows, we adopt the ''lamellar'' picture[70,69] illustrated in Fig. 1. Specifically, the system is defined to include the finite lamella of fluid bounded by imaginary planes at $x=0$, $x=s_x$, $y=0$, $y=s_y$, $z=0$, and $z=L$. The remainder of the fluid film (which is infinite in the transverse directions) and the confining walls constitute the surroundings. We focus on the case where the upper and lower walls are molecularly smooth, identical and rigid. The description *molecularly smooth*, in this context, implies that the confining plates lack structure and, consequently, cannot be used to shear the fluid film. The independent variables describing the finite lamella are thus in principle S, N, s_x, s_y, and L.

The differential form of the fundamental equation for the finite lamella is given by

$$dU = TdS - dW_{\mathrm{mech}} + \mu dN, \tag{2.1}$$

where T is the temperature, μ is the chemical potential, and dW_{mech} represents the mechanical work done by the lamellar system on its surroundings. From Fig. 1, it can be deduced that this work can be expressed in terms of normal stresses,

$$dW_{\mathrm{mech}} = -\sigma_{xx} s_y L ds_x - \sigma_{yy} s_x L ds_y - \sigma_{zz} s_x s_y dL. \tag{2.2}$$

Here σ_{ij} is the ij component of the total stress tensor ($i,j = x,y,z$) and ds_j is a displacement in the j direction. Note that σ_{ij} is simply the average of the j component of the stress applied to the i-directed face. The sign convention is such that if the force exerted by the lamella on the i-directed face points outward, σ_{ij} is negative, or, equivalently, the work is positive if done *by* the lamella *on* the surroundings.

Substituting Eq. (2.2) into Eq. (2.1) yields

$$dU = TdS + \sigma_{xx} s_y L ds_x + \sigma_{yy} s_x L ds_y + \sigma_{zz} s_x s_y dL + \mu dN. \tag{2.3}$$

Since the lamella is homogeneous and isotropic in any $x-y$ plane, the transverse components of the stress tensor are identical (i.e., $\sigma_{xx} = \sigma_{yy}$). Thus, upon introduction of the area $A = s_x s_y$ (of the z-directed face) as an independent variable and the transverse and normal components of the pressure tensor ($P_{\parallel} = -\sigma_{xx} = -\sigma_{yy}$, $P_{zz} = -\sigma_{zz}$), the fundamental equation becomes

$$dU = TdS - P_{\parallel} L dA - P_{zz} A dL + \mu dN. \tag{2.4}$$

As one might expect, in the limit $L \to \infty$, we have $P_{\parallel}$, $P_{zz} \to P^{\mathrm{bulk}}$, where P^{bulk} is the bulk pressure.

Alternative thermodynamic potentials can be derived from the fundamental equation (2.4) in the usual way via Legendre transforms. For instance, the Helmholtz free energy F is given by

$$dF = d(U - TS) = -SdT - P_{\parallel} L dA - P_{zz} A dL + \mu dN. \tag{2.5}$$

Similarly, we can derive relationships for the generalized enthalpy H,

$$dH = d(U + P_{\parallel} AL) = TdS + AL dP_{\parallel} - (P_{zz} - P_{\parallel}) A dL + \mu dN, \tag{2.6}$$

the generalized Gibbs free energy G,

$$dG = d(F + P_{\parallel} AL) = -SdT + AL dP_{\parallel} - (P_{zz} - P_{\parallel}) A dL + \mu dN, \tag{2.7}$$

and the grand potential Ω,

$$d\Omega = d(F - \mu N) = -SdT - P_{\parallel} L dA - P_{zz} A dL - N d\mu. \tag{2.8}$$

The uniformity of the film in the transverse directions also implies that $P_{\parallel}$ is independent of A for fixed pore width L, temperature T, and chemical potential μ. Hence, it can be seen from Eq. (2.4) that U is a homogeneous function of degree one in S, N, and A. Euler's theorem allows direct integration of Eq. (2.4) to yield

$$U = TS + \mu N - P_{\parallel} LA. \tag{2.9}$$

From Eq. (2.9), expressions for the Helmholtz free energy F,

$$F = U - TS = \mu N - P_{\parallel} LA, \tag{2.10}$$

the enthalpy H,

$$H = U + P_{\parallel} AL = \mu N + TS, \tag{2.11}$$

the Gibbs free energy G,

$$G = F + P_{\parallel} AL = \mu N, \tag{2.12}$$

and the grand potential Ω,

$$\Omega = F - \mu N = -P_{\parallel} LA \tag{2.13}$$

follow.

Response functions[71] can be obtained by differentiation of the thermodynamic potentials presented above. We thus have the mixed stress–strain expansivity $\alpha_{\parallel}$,

$$\alpha_{\parallel}=\frac{1}{AL}\left[\frac{\partial(\partial G/\partial P_{\parallel})_{T,N,L}}{\partial T}\right]_{P_{\parallel},N,L}=-\left(\frac{\partial \ln \rho_p}{\partial T}\right)_{P_{\parallel},L}, \tag{2.14}$$

the mixed stress-strain isothermal compressibility $\kappa_{\parallel}$,

$$\kappa_{\parallel}=-\frac{1}{AL}\left(\frac{\partial^2 G}{\partial P_{\parallel}^2}\right)_{T,N,L}=\left(\frac{\partial \ln \rho_p}{\partial P_{\parallel}}\right)_{T,L}, \tag{2.15}$$

and the isostress molar heat capacity $c_{\parallel}$,

$$c_{\parallel}=\left(\frac{\partial(H/N)}{\partial T}\right)_{P_{\parallel},L}=T\left(\frac{\partial(S/N)}{\partial T}\right)_{P_{\parallel},L}, \tag{2.16}$$

where $\rho_p=N/AL$ is the overall number density in the pore. In taking the limit $L\to\infty$, we recover the bulk thermodynamic response functions ($\alpha_{\parallel}\to\alpha_P$, $\kappa_{\parallel}\to\kappa_T$, and $c_{\parallel}\to c_P$).

In order to investigate the effect of confinement on the phase behavior of a fluid film, it is useful to develop the thermodynamic criteria for equilibrium of coexisting fluid phases. In Appendix A it is shown that the appropriate conditions for coexistence of two fluid phases denoted by$^{(1)}$ and$^{(2)}$ in a slit-pore of fixed width L that is in equilibrium with a bulk fluid (at $T^{\text{bulk}},\mu^{\text{bulk}}$) are given by

$$\begin{aligned} T^{\text{bulk}}&=T^{(1)}=T^{(2)},\\ \mu^{\text{bulk}}&=\mu^{(1)}=\mu^{(2)},\\ P_{\parallel}^{(1)}&=P_{\parallel}^{(2)}. \end{aligned} \tag{2.17}$$

In Sec. III, the above relations are used to investigate the thermodynamics of a waterlike model fluid in thin-film confinement.

III. MICROSCOPIC FORMULATION

In this section, we develop a microscopic perturbation theory for an associating fluid that is confined between two parallel substrates. Our approach is based on the work of Schoen and Diestler,[61] which we extend to include hydrogen bonding interactions between fluid molecules. The total potential energy in this system Φ is given by the sum of the contributions from the fluid–wall and fluid–fluid interactions, Φ_{fw} and Φ_f,

$$\Phi=\Phi_{fw}+\Phi_f. \tag{3.1}$$

As is standard of perturbation theories for the liquid state,[72] the fluid–fluid and fluid–wall interactions are divided into repulsive ($\mathcal{R}$) and attractive ($\mathcal{A}$) contributions,

$$\begin{aligned} \Phi_f&=\Phi_f^{\mathcal{R}}+\Phi_f^{\mathcal{A}},\\ \Phi_{fw}&=\Phi_{fw}^{\mathcal{R}}+\Phi_{fw}^{\mathcal{A}}. \end{aligned} \tag{3.2}$$

We treat the short-ranged repulsive fluid–fluid and fluid–wall contributions as hard-sphere interactions, i.e.,

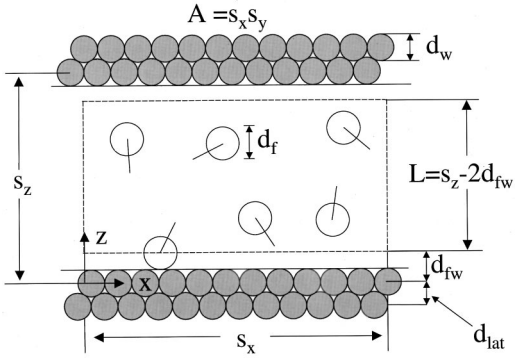

FIG. 2. Schematic of an associating fluid (white molecules) confined between parallel crystalline substrates (dark molecules). The bonding arms extending from the fluid molecules indicate the orientation-dependent nature of the fluid-fluid interactions. Although only two crystalline planes of molecules are shown in each substrate, the substrates actually comprise two infinite half-spaces ($z\leqslant 0$ and $z\geqslant s_z$) of such molecular planes.

$$\begin{aligned} \Phi_f^{\mathcal{R}}&=\sum_{i=1}^{N-1}\sum_{j=i+1}^{N}u_f^{\text{HS}}(r_{ij}),\\ \Phi_{fw}^{\mathcal{R}}&=\sum_{j=1}^{N}\sum_{k=1}^{N^{\text{sub}}}u_{fw}^{\text{HS}}(r_{jk}), \end{aligned} \tag{3.3}$$

where $u_f^{\text{HS}}(r_{ij})$ is given by

$$u_f^{\text{HS}}(r_{ij})=\begin{cases}0 & r_{ij}>d_f\\ \infty & r_{ij}\leqslant d_f\end{cases}, \tag{3.4}$$

and $u_{fw}^{\text{HS}}(r_{jk})$ is given by

$$u_{fw}^{\text{HS}}(r_{jk})=\begin{cases}0 & r_{jk}>d_{fw}\\ \infty & r_{jk}\leqslant d_{fw}\end{cases}. \tag{3.5}$$

Here, r_{ij} is the distance between the centers of fluid molecules i and j, r_{jk} is the distance between the centers of a fluid molecule j and a substrate molecule k, N is the total number of molecules in the fluid, N^{sub} is the total number of molecules in the substrates, d_f is the diameter of a fluid molecule, d_w is the diameter of a substrate molecule, and $d_{fw}=(d_f+d_w)/2$.

As a useful simplification[61] consistent with the thermodynamic formalism developed in the previous section, we choose to ''smear'' the repulsive interaction in the surface layer of the confining substrates to generate two smooth hard walls (see Fig. 2). These hard walls bound a rectangular slit of width $L=s_z-2d_{fw}$ that is ''accessible'' to the centers of the fluid molecules. The modified fluid–wall repulsive interaction u_{fw}^{HS} is thus

$$u_{fw}^{\text{HS}}(z_i)=\begin{cases}0 & d_{fw}<z_i<s_z-d_{fw}\\ \infty & \text{otherwise}\end{cases}. \tag{3.6}$$

Here, z_i is the z-coordinate of the ith fluid molecule. For the attractive interactions between molecules in the fluid (j) and molecules in the substrate (k), we use

$$\Phi_{fw}^{\mathcal{A}}=\Phi_{fw}^{\text{disp}}=\sum_{j=1}^{N}\sum_{k=1}^{N^{\text{sub}}}u_{fw}^{\text{disp}}(r_{jk}), \tag{3.7}$$

where $\Phi_{fw}^{\rm disp}$ is the fluid–wall dispersion interaction, $u_{fw}^{\rm disp}(r_{jk})$ is given by

$$u_{fw}^{\rm disp}(r_{jk}) = -4\epsilon_{fw}\left(\frac{d_{fw}}{r_{jk}}\right)^6, \tag{3.8}$$

and ϵ_{fw} is the familiar Lennard-Jones energetic parameter. Note that even though the substrate has attractive interactions with the fluid, it is hydrophobic in the sense that it cannot participate in hydrogen bonds with the fluid molecules.

Consistent with the ''smearing'' of the repulsive fluid–substrate interactions, we average the attractive contribution of the fluid–substrate interaction $-4\epsilon_{fw}(d_{fw}/r_{jk})^6$ over the (x,y) positions of substrate molecules in the planes in which they lie. If we then treat each substrate as an infinite half-space of molecular planes and approximate the sum over planes by the Euler–Maclaurin formula,[73] we obtain a fluid–wall potential that depends only on the z-coordinates of the fluid molecules,[61]

$$\Phi_{fw} = \sum_{i=1}^{N} u_{fw}^{\rm HS}(z_i) + u_{fw}^{\rm disp}(z_i), \tag{3.9}$$

where

$$u_{fw}^{\rm disp}(z_i) = -\frac{2\pi\rho_w\epsilon_{fw}d_{fw}^6}{3d_{\rm lat}}[z_i^{-3} + (s_z - z_i)^{-3}]. \tag{3.10}$$

In the above equation, ρ_w is the areal number density in a plane of the substrate and $d_{\rm lat}$ is the spacing between neighboring substrate planes (Fig. 2). For the purposes of this study, we take the substrate to be a close-packed fcc lattice, i.e., $\rho_w d_w^2 = 2/\sqrt{3}$ and $d_{\rm lat} = d_w/\sqrt{2}$.

For the attractive fluid–fluid interactions, we use

$$\Phi_f^A = \Phi_f^{\rm HB} + \Phi_f^{\rm disp}, \tag{3.11}$$

where $\Phi_f^{\rm disp}$ is the dispersion contribution,

$$\Phi_f^{\rm disp} = \sum_{i=1}^{N-1}\sum_{j=i+1}^{N} u_f^{\rm disp}(r_{ij}), \tag{3.12}$$

and $u_f^{\rm disp}(r_{ij})$ is given by

$$u_f^{\rm disp}(r_{ij}) = -4\epsilon_f\left(\frac{d_f}{r_{ij}}\right)^6. \tag{3.13}$$

Here, ϵ_f is the fluid–fluid Lennard-Jones energetic parameter and $\Phi_f^{\rm HB}$ is the energy associated with hydrogen bonds formed between fluid molecules, which will be discussed shortly.

The combination of Eqs. (3.1), (3.2), (3.3), (3.6), (3.9), and (3.11) yields the following expression for the potential energy Φ;

$$\Phi = \Phi_p^{\rm HS} + \Phi_f^{\rm HB} + \Phi_f^{\rm disp} + \Phi_{fw}^{\rm disp}, \tag{3.14}$$

where $\Phi_p^{\rm HS}$ represents the potential energy of a fluid of hard spheres with diameter d_f whose centers are confined by parallel hard walls to a slit of width $L = s_z - 2d_{fw}$, i.e.,

$$\Phi_p^{\rm HS} = \sum_{i=1}^{N-1}\sum_{j=i+1}^{N} u_f^{\rm HS}(r_{ij}) + \sum_{i=1}^{N} u_{fw}^{\rm HS}(z_i). \tag{3.15}$$

This confined hard-sphere system will serve as the reference fluid for the perturbation analysis presented below.

The connection between microscopic interactions and equilibrium thermodynamics is established through the canonical partition function Q,[74]

$$Q = \left(\frac{1}{N!\Lambda^{3N}}\right)\int\int d\mathbf{r}^N d\omega^N \exp(-\beta\Phi), \tag{3.16}$$

from which the Helmholtz free energy is obtained, $F = -\beta^{-1}\ln Q$. Here, $\beta = 1/k_BT$, k_B is Boltzmann's constant, T is the temperature, and N is the number of molecules. The integration in Eq. (3.16) is carried out over the vector of accessible positions $\mathbf{r}^N = \{\mathbf{r}_1, \mathbf{r}_2, \ldots, \mathbf{r}_N\}$ and molecular orientations $\omega^N = \{\omega_1, \omega_2, \ldots, \omega_N\}$ in the pore. For a monatomic species, Λ is the familiar thermal wavelength. For polyatomic molecules, Λ is generalized to include contributions from relevant internal degrees of freedom; however, it exhibits no pressure or density dependence.

Substitution of Eq. (3.14) into Eq. (3.16) yields

$$Q = \left(\frac{1}{N!\Lambda^{3N}}\right)\int\int d\mathbf{r}^N d\omega^N \times \exp[-\beta(\Phi_p^{\rm HS} + \Phi_f^{\rm HB} + \Phi_f^{\rm disp} + \Phi_{fw}^{\rm disp})]. \tag{3.17}$$

Multiplying and dividing by the configurational partition function for the confined hard sphere fluid $Z_p^{\rm HS}$, which is given by

$$Z_p^{\rm HS} = \int d\mathbf{r}^N \exp(-\beta\Phi_p^{\rm HS}), \tag{3.18}$$

allows the integrals appearing in Eq. (3.17) to be rewritten as

$$\int d\mathbf{r}^N \exp(-\beta\Phi_p^{\rm HS}) \times \frac{\int\int d\mathbf{r}^N d\omega^N \exp[-\beta(\Phi_p^{\rm HS} + \Phi_f^{\rm HB} + \Phi_f^{\rm disp} + \Phi_{fw}^{\rm disp})]}{\int d\mathbf{r}^N \exp(-\beta\Phi_p^{\rm HS})} = Z_p^{\rm HS}\cdot\int d\omega^N \langle \exp[-\beta(\Phi_f^{\rm HB} + \Phi_f^{\rm disp} + \Phi_{fw}^{\rm disp})]\rangle_p^{\rm HS}. \tag{3.19}$$

Note that this transformation is exact. The notation $\langle\cdots\rangle_p^{\rm HS}$ in the right-hand member of Eq. (3.19) indicates that the average is to be taken in the ''confined hard-sphere'' ensemble. This implies sampling all possible configurations of N hard spheres with diameter d_f whose centers are confined to a slit of width $L = s_z - 2d_{fw}$, and calculating, for each such configuration, the value of $\exp(-\beta[\Phi_f^{\rm HB} + \Phi_f^{\rm disp} + \Phi_{fw}^{\rm disp}])$ by ''turning on'' the dispersion attractions and hydrogen bonds with fixed molecular orientation. The integral is then taken over all possible sets of orientations.

The combination of Eqs. (3.17) and (3.19) allows the Helmholtz free energy F to be expressed as

$$F=-\beta^{-1}\ln\left[\frac{Z_p^{\mathrm{HS}}}{N!\lambda^{3N}}\right]-\beta^{-1}\times\ln\left[\int d\omega^N\langle\exp(-\beta[\Phi_f^{\mathrm{HB}}+\Phi_f^{\mathrm{disp}}+\Phi_{fw}^{\mathrm{disp}}])\rangle_p^{\mathrm{HS}}\right]. \tag{3.20}$$

To evaluate the integrand, we recall the cumulant expansion[75] for a general random variable x,

$$\langle\exp(cx)\rangle=\exp\left[c\langle x\rangle+\frac{c^2}{2!}(\langle x^2\rangle-\langle x\rangle^2)+\cdots\right]. \tag{3.21}$$

We determine the average in Eq. (3.20) approximately by neglecting fluctuations. Explicitly, we neglect second and all higher order cumulants

$$\langle\exp(-\beta[\Phi_f^{\mathrm{HB}}+\Phi_f^{\mathrm{disp}}+\Phi_{fw}^{\mathrm{disp}}])\rangle_p^{\mathrm{HS}}\approx\exp\langle-\beta[\Phi_f^{\mathrm{HB}}+\Phi_f^{\mathrm{disp}}+\Phi_{fw}^{\mathrm{disp}}]\rangle_p^{\mathrm{HS}}. \tag{3.22}$$

Substituting Eq. (3.22) into Eq. (3.20) yields the following expression for the Helmholtz free energy F,

$$F=-\beta^{-1}\ln\left[\frac{Z_p^{\mathrm{HS}}}{N!\lambda^{3N}}\right]+\langle\Phi_f^{\mathrm{disp}}\rangle_p^{\mathrm{HS}}+\langle\Phi_{fw}^{\mathrm{disp}}\rangle_p^{\mathrm{HS}}-\beta^{-1}\ln\left[\int d\omega^N\exp\langle-\beta\Phi_f^{\mathrm{HB}}\rangle_p^{\mathrm{HS}}\right]. \tag{3.23}$$

The dispersion interactions are expected to play only a minor role in the structuring of molecules in the dense fluid and, consequently, are often modeled as uniform, attractive background potentials. In fact, Schoen and Diestler[61] have demonstrated that mean-field approximations of this nature can be computed for the dispersion interactions in the slit geometry shown in Fig. 2. Specifically, by assuming that the fluid-fluid radial distribution function $g(\mathbf{r}_1,\mathbf{r}_2)$ has the form,

$$g(\mathbf{r}_1,\mathbf{r}_2)=\begin{cases}0 & |\mathbf{r}_2-\mathbf{r}_1|<d_f\\ 1 & |\mathbf{r}_2-\mathbf{r}_1|\geqslant d_f\end{cases}, \tag{3.24}$$

the energetic contributions from the dispersion interactions can be obtained by integrating Eq. (3.10) with respect to z_i and Eq. (3.13) with respect to r_{ij} and the lamellar volume. The resulting mean-field averages are[61]

$$\langle\Phi_{fw}^{\mathrm{disp}}\rangle_p^{\mathrm{HS}}=\left\langle\sum_{i=1}^{N}u_{fw}^{\mathrm{disp}}(z_i)\right\rangle_p^{\mathrm{HS}} \tag{3.25}$$

$$=-\frac{2N\pi\rho_w\epsilon_{fw}d_{fw}^3}{3d_{\mathrm{lat}}}\left[\frac{1}{\zeta}-\frac{1}{\zeta(\zeta+1)^2}\right]=-N\Psi_0\left[\frac{1}{\zeta}-\frac{1}{\zeta(\zeta+1)^2}\right]=-N\Psi_p(\zeta),\quad \zeta>0, \tag{3.26}$$

and

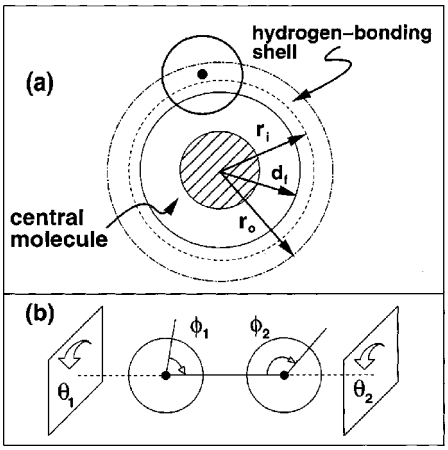

FIG. 3. Microscopic model of a fluid with orientation-dependent interactions. (a) Molecules have a hard core of diameter d_f, and are therefore surrounded by an exclusion sphere of radius d_f, within which the center of no other molecule can penetrate. In order to form a hydrogen bond, a central molecule must be surrounded by an empty cavity of radius r_i (here $r_i\approx d_f$), and a second molecule must be inside its hydrogen bonding shell $r_i\leqslant r\leqslant r_o$. (b) In addition, the two participating molecules must be properly oriented, with their bonding directions pointing towards each other ($\phi_1,\phi_2\leqslant\phi^*$), regardless of the value of θ_1 and θ_2. The presence of additional molecules inside the hydrogen bonding shell weakens an existing bond.

$$\langle\Phi_f^{\mathrm{disp}}\rangle_p^{\mathrm{HS}}=\left\langle\sum_{i=1}^{N-1}\sum_{j=i+1}^{N}u_f^{\mathrm{disp}}(r_{ij})\right\rangle_p^{\mathrm{HS}} \tag{3.27}$$

$$=-\frac{8N\pi\epsilon_f d_f^3}{3}\left[1-\frac{3(d_f/d_{fw})}{4\zeta}+\frac{(d_f/d_{fw})^3}{8\zeta^3}\right]\rho_p=-Na^{\mathrm{bulk}}\left[1-\frac{3(d_f/d_{fw})}{4\zeta}+\frac{(d_f/d_{fw})^3}{8\zeta^3}\right]\rho_p=-Na_p(\zeta)\rho_p,\qquad \zeta>2d_f/d_{fw}, \tag{3.28}$$

where $\zeta=L/d_{fw}=(s_z-2d_{fw})/d_{fw}$ is a dimensionless pore width, $\rho_p=N/AL=N/(Ad_{fw}\zeta)$ is the mean number density in the pore, and a^{bulk} is the dispersion interaction parameter for the bulk van der Waals fluid.

To model the hydrogen-bonding interactions in the fluid Φ_f^{HB}, we appeal to a recently introduced model for association[42] that is able to capture the distinctive thermodynamic properties of bulk liquid water, including density maxima, compressibility and specific heat minima, sharp increases in the response functions at low temperatures, and the possibility of a polyamorphic phase transition between a high-density and a low-density fluid. Within the context of this model, a hydrogen bond may form between two molecules if several geometric criteria[42] are met. These criteria are designed to capture the minimal features of hydrogen-bond interactions in liquid water; namely, the molecules involved must possess mutually favorable orientation (low orientational entropy), and an open, low-density environment must exist in the vicinity of the bond. These basic physical attributes of the hydrogen bond are modeled as follows (see Fig. 3):

(1) One of the two participating molecules must have a cavity of radius r_i, empty of any molecular centers, surrounding it (we term this the *central molecule* of the pair);
(2) The pair must be separated by a distance r that lies within the *hydrogen-bonding shell* of the central molecule, with $r_i \leqslant r \leqslant r_o$;
(3) The pair must exhibit mutually favorable orientation, $\phi_1,\ \phi_2 \leqslant \phi^*$;
(4) The presence of additional molecules in the hydrogen-bonding shell ''crowds'' and thereby weakens the existing bond. We assign a strength $-\epsilon_{\max}$ to a hydrogen bond and a penalty ϵ_{pen} for each nonbonding molecule in the hydrogen-bonding shell.

In this study, we take $-\epsilon_{\max}=-23$ kJ/mol and $\epsilon_{\text{pen}}=3$ kJ/mol. It follows that if more than seven nonbonding molecules are contained in the hydrogen-bonding shell, the central molecule is not available for bonding.

These geometric criteria are designed to model, albeit in a rudimentary fashion, specific features of the hydrogen-bond interaction. For instance, the requirement of a cavity of radius r_i surrounding the central molecule promotes a low-density, open environment in the vicinity of the bonded pair. Criterion (2) defines the largest allowable separation r_o for molecular centers participating in a hydrogen bond. Indeed, the shell $(r_i \leqslant r \leqslant r_o)$ physically represents the width of the distribution of bond lengths in the model substance. For perspective, typical bond lengths in $(H_2O)_2$ measured in the vapor phase (2.98 Å) are roughly 8% larger than the observed distance in ice.[76] Criterion (3) constrains the bonding sites on each molecule to lie within an angle ϕ^* of the line connecting molecular centers. The magnitude of ϕ^* determines the freedom of alignment between molecular sites, and thus is necessarily related to the reduction of orientational entropy upon bonding. As has been demonstrated,[42] minor alterations in the geometric ''librational'' and ''vibrational'' bonding constraints, as defined by (r_i, r_o, ϕ^*), can result in dramatic changes in the macroscopic phase behavior of the system. Criterion (4) prescribes the dependence of the hydrogen-bond energy $-\epsilon_j$ on its local structural environment,

$$-\epsilon_j = -\epsilon_{\max} + (j-1)\epsilon_{\text{pen}}, \tag{3.29}$$

where $j-1$ is the number of nonbonded molecules in the hydrogen-bonding shell of the central molecule. This crowding rule is a simple model for the fact that hydrogen bonding is a many-body interaction, i.e., the presence of nonbonding neighbors can severely disrupt the electronic structure of the bonded pair.

Clearly, these criteria oversimplify the microscopic details of the hydrogen bond. For instance, this coarse description will not promote many of the microscopic, structural details characteristic of liquid water that distinguish its behavior from that of ''simple'' fluids, e.g., the interplay in water between translational and tetrahedral ordering.[77] Nevertheless, the model is able to capture the highly nontrivial thermodynamic consequences of directional bonding.[42]

An expression for the hydrogen-bonding contribution to the Helmholtz free energy F has been derived[42] for this model in the bulk, uniform fluid. The appropriate reference fluid for that system is the uniform hard-sphere fluid. In contrast, the appropriate reference fluid for the present thin-film confinement model is an inhomogeneous hard-sphere fluid confined between hard walls. Noting this difference in reference system, the derivation of hydrogen-bonding contribution to F [i.e., the last term of Eq. (3.23)] follows directly from the original treatment,[42] and we arrive at

$$-\beta^{-1}\ln\left[\int d\omega^N \exp\langle -\beta\Phi_f^{\text{HB}}\rangle_p^{\text{HS}}\right] \approx -N\beta^{-1}\left[\ln(4\pi)+\sum_{j=1}^{8} p_j^{\text{pore}}(\rho_p,\zeta)\ln f_j\right]. \tag{3.30}$$

The reader is referred to that paper for a more detailed discussion. Here, f_j is given by

$$f_j=\left[1+\frac{j}{4}(1-\cos\phi^*)^2(\exp\{\beta\epsilon_j\}-1)\right]. \tag{3.31}$$

The function $p_j^{\text{pore}}(\rho_p,\zeta)$ represents the probability that, in a confined hard-sphere fluid at a density ρ_p, a given hard sphere has a cavity of radius r_i surrounding it and that j other sphere centers lie within its hydrogen-bonding shell (see Fig. 3). This is tantamount to stating that a hard sphere meets the positional (if not the orientational) requirements for hydrogen-bonding to one of its j neighbors. We note that $p_j^{\text{pore}}(\rho_p,\zeta)$ generally depends on all of the n-body molecular correlation functions $g^{(n)}(\mathbf{r}^n)$ for the confined hard-sphere fluid. Indeed, the method for determining $p_j^{\text{pore}}(\rho_p,\zeta)$ will determine the ''level'' of the theory and will be discussed in detail in the next section.

If we assume the simplest approximation for the configurational partition function of the confined hard-sphere fluid $Z_p^{\text{HS}}=[Ad_{fw}\zeta - Nb_p(\zeta)]^N$, exact only in one dimension, then the Helmholtz free energy F given by Eqs. (3.23), (3.26), (3.28), and (3.30) becomes

$$F=-N\beta^{-1}\left[\ln\left(\frac{1-\rho_p b_p(\zeta)}{\rho_p\lambda^3}\right)+1\right]-Na_p(\zeta)\rho_p - N\Psi_p(\zeta)-N\beta^{-1}\left[\ln(4\pi)+\sum_{j=1}^{8} p_j^{\text{pore}}(\rho_p,\zeta)\ln f_j\right]. \tag{3.32}$$

Here, $b_p(\zeta)$ is the familiar van der Waals excluded-volume parameter that sets the maximum number density $\rho_p^{\max}(\zeta)$ that the hard-sphere reference fluid can attain in the slit pore.

To ensure that the slit-pore free energy F matches, in the limit $\zeta\to\infty$, the previously derived expression for the free energy of the bulk associating fluid,[42] we set

$$b_p(\zeta)=\frac{1}{\rho_p^{\max}(\zeta)}=\frac{1}{\rho_p[\eta_p=0.64]}, \tag{3.33}$$

where $\rho_p[\eta_p=0.64]$ is the pore density at which the mean packing fraction η_p in the pore attains the value $\eta_p=0.64$, historically termed the random close-packed state.[78] In the slit-pore geometry, the mean packing fraction η_p can be related to the density profile $\rho(z)$, the form of which is gener-

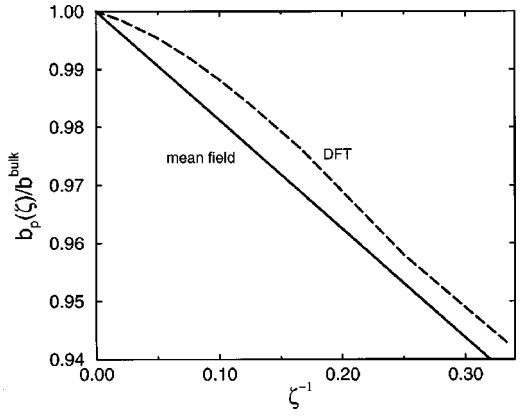

FIG. 4. Normalized excluded-volume parameter $b_p(\zeta)/b^{\text{bulk}}$ plotted vs inverse pore width ζ^{-1}. Shown are the quantities as determined by the mean-field expression in Eq. (3.36) (solid line) and the density functional theory outlined in Appendix B (dashed line).

ally determined from a molecular simulation or a density functional theory (see Appendix B). That relationship is shown in Appendix C to be given by

$$\eta_p=(s_z-2d_{fw})^{-1}\int_{d_{fw}}^{s_z-d_{fw}}dz\int_{z-d_f/2}^{z+d_f/2}dz'\,\rho(z')\,\pi\times\left[\left(\frac{d_f}{2}\right)^2-(z-z')^2\right], \tag{3.34}$$

and the average pore density ρ_p is simply

$$\rho_p=(s_z-2d_{fw})^{-1}\int_{d_{fw}}^{s_z-d_{fw}}dz\,\rho(z)=N/AL=N/[A\zeta d_{fw}]. \tag{3.35}$$

In this investigation, we examine two approximate methods for determining the relationship between ρ_p and the mean packing fraction η_p for the confined (hard-sphere) reference fluid. The first method is a mean-field approach, which assumes that the fluid film is homogeneous [i.e., $\rho(z)=\rho_p$ for $d_{fw}<z<s_z-d_{fw}$ and $\rho(z)=0$ otherwise]. Substituting this density profile into Eq. (3.34) yields the simple result

$$\eta_p=\frac{\pi d_f^3\rho_p}{6}\left[1-\frac{3}{16\zeta}\right], \tag{3.36}$$

which implies,

$$b_p(\zeta)=\frac{\pi d_f^3}{6(0.64)}\left[1-\frac{3}{16\zeta}\right]=b^{\text{bulk}}\left[1-\frac{3}{16\zeta}\right]. \tag{3.37}$$

The second method that we examine for determining η_p accounts for the structure of the inhomogeneous reference fluid by employing a density functional theory (DFT) for hard spheres in confinement (outlined in Appendix B). The density profile $\rho(z)$ generated by the DFT is then substituted into Eq. (3.34) to determine η_p, and the excluded-volume parameter $b_p(\zeta)$ can be determined from Eq. (3.33). Figure 4 compares the dependence of the ratio $b_p(\zeta)/b^{\text{bulk}}$ upon the inverse pore width, as calculated via the mean-field expression (3.36) and by density functional theory (Appendix B).

The important point is that both approaches predict that $b_p(\zeta)$ decreases with increasing confinement. This indicates that the parallel confining walls have the effect of reducing the local packing fraction (and hence the average coordination number) in the film relative to the bulk fluid at the same number density. This can be easily understood, given that the fraction of molecules whose coordination numbers are ''sterically-hindered'' by their proximity to the wall increases with decreasing ζ. The implications of this purely geometrical effect for the thermodynamics of an associating fluid are investigated in the mean-field theory presented in the next section.

From Eqs. (2.5) and (3.32), we see that differentiation of F yields the transverse component of the pressure tensor $P_\parallel$,

$$P_\parallel=\rho_p^2\left(\frac{\partial F/N}{\partial\rho_p}\right)_{T,N,L}=\frac{\rho_p}{\beta[1-\rho_p b_p(\zeta)]}-a_p(\zeta)\rho_p^2-\frac{\rho_p^2}{\beta}\sum_{j=1}^{8}\left(\frac{\partial p_j^{\text{pore}}(\rho_p)}{\partial\rho_p}\right)_{T,\zeta}\ln f_j. \tag{3.38}$$

Here, it is useful to note that the transverse pressure $P_\parallel$, unlike F, is independent of the strength of the fluid–wall dispersion interaction $\Psi_p(\zeta)$.

To complete the theory we need a strategy for analyzing the probability functions $p_j^{\text{pore}}(\rho_p,\zeta)$ for the hard-sphere reference fluid in confinement. In Sec. IV, the hard-sphere statistics are examined with two different levels of approximation, a homogeneous (mean-field) theory and an inhomogeneous (DFT) approach.

IV. RESULTS AND DISCUSSION

In order to analyze the thermodynamics and phase behavior of the thin film, we need to obtain an expression for the hard-sphere probability function $p_j^{\text{pore}}(\rho_p,\zeta)$. Recall that $p_j^{\text{pore}}(\rho_p,\zeta)$ represents the probability that, in a confined hard-sphere fluid at a density ρ_p, a given sphere center has a cavity of radius r_i surrounding it and that j other sphere centers lie within its hydrogen-bonding shell (shown in Fig. 3).

Using statistical geometric arguments, the following approximate relationship for the probability function that describes the bulk fluid p_j^{bulk} has been derived,[42]

$$p_j^{\text{bulk}}=\exp\left[-\frac{24\eta}{d_f^3}\int_{d_f}^{r_i}r^2G(r)dr\right]\times\frac{1}{j!}\left(\frac{24\eta}{d_f^3}\int_{d_f}^{r_o}r^2G(r)dr\right)^j\times\exp\left[-\frac{24\eta}{d_f^3}\int_{d_f}^{r_o}r^2G(r)dr\right], \tag{4.1}$$

where $\eta=\pi d_f^3\rho/6$ represents the bulk packing fraction. In Eq. (4.1), the quantity $G(r)$ is the *conditional pair-distribution function*, defined such that the product $\rho G(r)$ yields the concentration of sphere centers located a distance r away from a hard-sphere center, given that there are no sphere centers closer than r. This quantity plays an important

role in the scaled-particle theory[79] and, more generally, in the *statistical geometry* of liquids.[80–85] In the spirit of scaled-particle theory, Torquato[83] derived the following analytical approximation for $G(r)$:

$$G(r)=0 \quad r<d_f,$$
$$G(r)=a_0+\frac{a_1}{(r/d_f)}+\frac{a_2}{(r/d_f)^2} \quad r\geqslant d_f, \tag{4.2}$$

with

$$a_0=1+4\eta G(d_f),$$
$$a_1=\frac{3\eta-4}{2(1-\eta)}+2(1-3\eta)G(d_f),$$
$$a_2=\frac{2-\eta}{2(1-\eta)}+(2\eta-1)G(d_f), \tag{4.3}$$
$$G(d_f)=\frac{1-\eta/2}{(1-\eta)^3},$$

which can be directly substituted into Eq. (4.1). The analytical expression for p_j^{bulk} given by Eq. (4.1) is appealing because it approaches the exact result in the dilute limit when the cavity surrounding the central molecule is small ($\eta\to 0$, $r_i\to d_f$). Furthermore, we have found that the expression, while quantitatively accurate at low density, can capture many qualitative features of bulk hard-sphere statistics at higher packing fractions.

Below, we outline two approximate methods for determining the pore probability function $p_j^{\text{pore}}(\rho_p,\zeta)$, both of which utilize the analytical expression given in Eq. (4.1) for the bulk hard-sphere statistics.

A. Level 1: Homogeneous reference fluid

In the first level of approximation, we assume that the reference hard-sphere system confined between parallel walls is homogeneous [i.e., $\rho(z)=\rho_p$ for $d_{fw}<z<s_z-d_{fw}$ and $\rho(z)=0$ otherwise]. From Eq. (3.36), we see that this assumption implies that the mean packing fraction in the pore η_p is given by

$$\eta_p=\frac{\pi d_f^3\rho_p}{6}\left[1-\frac{3}{16\zeta}\right]. \tag{4.4}$$

We further assume that bulk hard-sphere statistics [as described by Eq. (4.1)] apply when evaluated at η_p, i.e.,

$$p_j^{\text{pore}}\approx p_j^{\text{bulk}}(\eta_p). \tag{4.5}$$

This expression, together with Eqs. (3.32), (3.29), (3.31), (3.26), (3.28), (3.37), (4.1), (4.2), (4.3), and (4.4) completes the mean-field associating fluid film theory.

Before analyzing the phase behavior of the associating fluid film in the mean-field theory, it is useful to consider the case where the hydrogen bonds are effectively ''turned off'' (i.e., $\epsilon_j=0,\forall j$). In this limit, the model reduces to a simple van der Waals (vdW) fluid confined between two parallel substrates, and the original perturbation theory of Schoen and Diestler[61] is recovered. This model, as is discussed extensively elsewhere,[61] qualitatively reproduces much of the phenomenology associated with sorption in mesoscopic porous materials.

The location of the critical point for the vdW pore fluid at a given pore width L can be determined analytically via the conditions,

$$\frac{1}{\rho_p}\left(\frac{\partial P_\parallel}{\partial\rho_p}\right)_{L,T=T_c}=\frac{1}{\rho_p}\frac{\partial}{\partial\rho_p}\left[\frac{1}{\rho_p}\left(\frac{\partial P_\parallel}{\partial\rho_p}\right)_{L,T=T_c}\right]_{L,T=T_c}=0. \tag{4.6}$$

The resulting expressions for the critical temperature T_c, the critical transverse pressure $P_{\parallel,c}$, and the critical pore density $\rho_{p,c}$ for the modified vapor–liquid transition in the confined vdW fluid are given by

$$T_c=\frac{8a_p(\zeta)}{27b_p(\zeta)k_B}\leqslant T_c^{\text{bulk}}=\frac{8a^{\text{bulk}}}{27b^{\text{bulk}}k_B},$$
$$P_{\parallel,c}=\frac{a_p(\zeta)}{27b_p^2(\zeta)}\leqslant P_c^{\text{bulk}}=\frac{a^{\text{bulk}}}{27(b^{\text{bulk}})^2}, \tag{4.7}$$
$$\rho_{p,c}=\frac{1}{3b_p(\zeta)}\geqslant\rho_c^{\text{bulk}}=\frac{1}{3b^{\text{bulk}}}.$$

The inequalities in Eq. (4.7) follow directly from Eqs. (3.28) and (3.37). Notice that the model predicts that confinement has the effect of depressing the critical temperature and critical pressure of the bulk ''vapor–liquid'' transition, while shifting the critical density to higher values. These results are in qualitative agreement with both experiments[86–92] and molecular simulations.[13,15]

We note that in the original formulation of the theory,[61] the excluded-volume parameter $b_p(\zeta)$ was taken to be a constant $b_p(\zeta)=b^{\text{bulk}}$, independent of pore width. This condition implies that the transverse pressure $P_\parallel$ diverges at the same number density $1/b^{\text{bulk}}$ for any degree of confinement. Unfortunately, it also implies that the critical density is completely unaffected by the pore width, i.e., $\rho_{p,c}=\rho_c^{\text{bulk}}$. Hence, accounting for the manner in which confinement affects the maximum attainable number density in the fluid, even in the crude mean-field fashion of Eq. (3.37), is important for generating qualitatively correct thermodynamic predictions.

In order to analyze the mean-field theory with hydrogen-bonding interactions, we must specify a total of seven fluid parameters ($r_i, r_o, \epsilon_{\max}, \epsilon_{\text{pen}}, \phi^*, d_f, a^{\text{bulk}}$) and three substrate parameters (d_w, Ψ_0, ζ). In the present work, we set the fluid parameters to values that reproduce the two-critical-point scenario in the bulk fluid.[42] Specifically, the magnitude of the maximum hydrogen-bond strength $\epsilon_{\max}$ and the hard-core diameter d_f are assigned the physically reasonable values of 23 kJ/mol and 3.11 Å, respectively. Recall that the crowding penalty ϵ_{pen}, is taken to be 3 kJ/mol per nonbonding molecule in the hydrogen-bonding-shell. The three parameters which describe the hydrogen-bond geometry are assigned the values $\phi^*=0.175$ radians, $r_i=1.01d_f$, $r_o=1.04d_f$. Furthermore, the dispersion interaction a^{bulk} is selected to be 0.269 $\text{Pam}^6\,\text{mol}^{-2}$, which essentially fixes the bulk vapor-liquid critical point at the correct experimental value of 647 K. This set of parameters reproduces the famil-

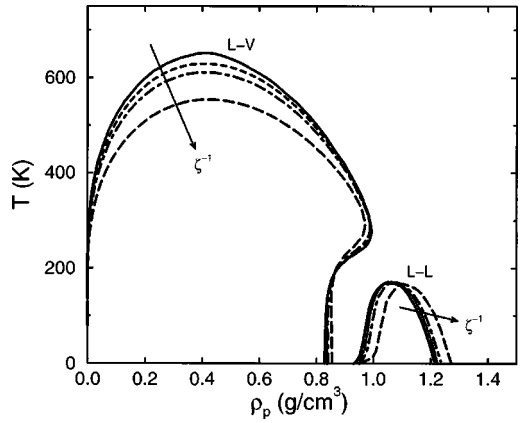

FIG. 5. The $T-\rho_p$ projection of the phase diagram for the associating fluid film in the mean-field theory. The curves represent loci of phase coexistence for the confinement-modified ''liquid–vapor'' ($L-V$) and ''liquid–liquid'' ($L-L$) transitions in pores of dimensionless width $\zeta=4$ (long-dashed), 10 (dotted–dashed), 20 (dashed), and ∞ (solid).

iar density maximum ($\rho=1$ g/cm^3) in the bulk fluid at 1 bar and 4 °C. Further details concerning the thermodynamics of the bulk system in the two-critical-point scenario are presented elsewhere.[42] For simplicity, the effective diameter of the substrate molecules d_w is taken to be identical to that of the fluid molecules $d_w=d_{fw}=d_f$. The effects of the dimensionless pore width $\zeta=L/d_{fw}$ and the strength of the fluid-wall attraction Ψ_0 [given by Eq. (3.26)] on the phase behavior and stability of the fluid film are examined below.

Figure 5 illustrates the $T-\rho_p$ projection of the phase diagram for the ''waterlike'' fluid film for various degrees of confinement, as determined by the mean-field theory. The curves represent loci of phase coexistence for the confinement-modified ''liquid–vapor'' ($L-V$) and ''liquid–liquid'' ($L-L$) transitions in pores of dimensionless width $\zeta=4$, 10, 20, and ∞ (corresponding to dimensional pore widths $\zeta d_{fw}\approx 1.2$ nm, 3.1 nm, 6.2 nm, and ∞, respectively). The arrows indicate that confinement shifts both critical points ($L-V$ and $L-L$) to lower temperature T and higher pore density ρ_p. A corresponding shift of the critical point to lower transverse pressure $P_\parallel$ occurs for the $L-V$ transition, while the $L-L$ critical point occurs at progressively higher transverse pressures as ζ is reduced (not shown). We recall that the equation of state of the fluid film given by Eq. (3.38) is independent of $\Psi_p(\zeta)$, rendering the global phase behaviors shown in Fig. 5 independent of the strength of the fluid–wall dispersion interaction.

The confinement-induced shifts in the location of the $L-V$ critical point for both the vdW fluid and the mean-field associating fluid are illustrated in Fig. 6 as a function of inverse pore width ζ^{-1}. Also shown is the relative shift in the location of the low-temperature $L-L$ critical point in the mean-field associating fluid. In the absence of hydrogen-bonding interactions, the analytical form for the critical point shift in the vdW fluid (i.e., $T_c-T_c^{\rm bulk}$, $P_{\parallel,c}-P_c^{\rm bulk}$, and $\rho_{p,c}-\rho_c^{\rm bulk}$) can be deduced from Eq. (4.7). In the case of the associating fluid film, the corresponding shifts ($L-V$ and $L-L$) are determined numerically by applying the criticality

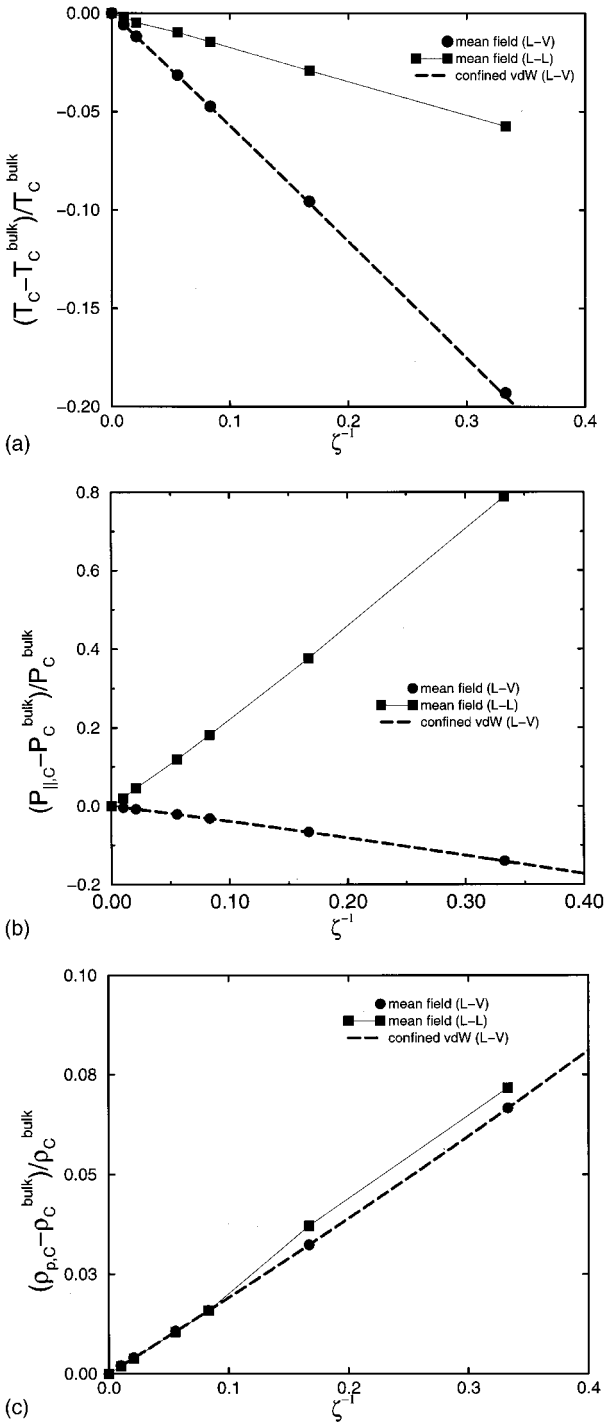

FIG. 6. Relative shifts for the liquid–vapor ($L-V$) and the liquid–liquid ($L-L$) critical points in the fluid film vs inverse pore width ζ^{-1}: (a) $(T_c-T_c^{\rm bulk})/T_c^{\rm bulk}$, (b) $(P_{\parallel,c}-P_c^{\rm bulk})/P_c^{\rm bulk}$, and (c) $(\rho_{p,c}-\rho_c^{\rm bulk})/\rho_c^{\rm bulk}$. Shown are results for the $L-V$ transition in the confined vdW fluid (dashed line) and the mean-field associating fluid (black circles). The relative shift for the $L-L$ transition in the associating fluid film (black squares) is also illustrated.

conditions in Eq. (4.6) to the equation of state given by Eq. (3.38).

By virtue of the slit-pore geometry, molecular correlation lengths can grow to infinity only in the transverse (x,y) directions. This means that while a true phase transition can occur in a slit pore, its criticality will correspond to the two-dimensional Ising universality class.[13] Nevertheless, Fisher

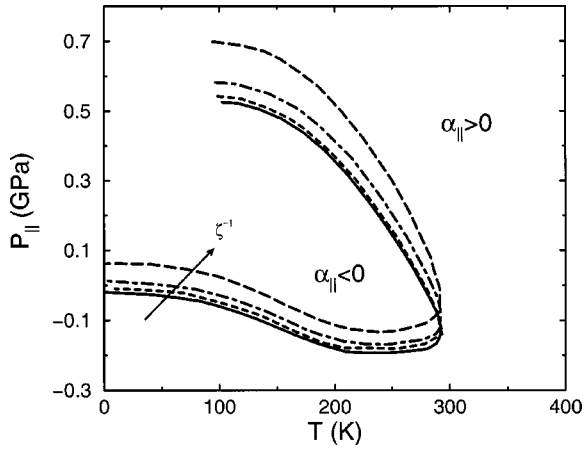

FIG. 7. The loci of state points for the associating fluid film in the $P_{\parallel}-T$ plane that satisfy $\alpha_{\parallel}=0$ (i.e. the TMD). Results are shown for pores of dimensionless width $\zeta=4$ (long-dashed), 10 (dotted-dashed), 20 (dashed), and ∞ (solid).

and Nakanishi[93] have employed scaling arguments to show that the shift in the $L-V$ critical temperature (for large slit pores) should obey

$$1-T_c/T_c^{\mathrm{bulk}}\propto\zeta^{-1/\nu}\quad\zeta\to\infty, \tag{4.8}$$

where $\nu\approx 0.63$ is the bulk three-dimensional correlation length exponent. On the other hand, calculations on a confined lattice gas model[94] have shown that the shift ($T_c^{\mathrm{bulk}}-T_c$) varies roughly as ζ^{-1} in the small-pore limit. As can be seen in Fig. 6, the magnitudes of the critical-point shifts for the vdW fluid ($L-V$) and the mean-field associating fluid ($L-V$ and $L-L$) also exhibit approximately linear variations with inverse pore width ζ^{-1}.

Two important points can be deduced from the critical point shifts shown in Fig. 6. First, the predicted trends for the $L-V$ critical point, while not quantitatively accurate, are in qualitative agreement with experiments and computer simulations on a number of pore fluids.[13,15] Second, the relative shifts in the $L-V$ critical points for the vdW fluid and the mean-field associating fluid are nearly identical. Thus, the energetically favorable hydrogen-bonding interactions, while important for the low-temperature behavior of the fluid, have little effect on the shift of the high-temperature $L-V$ critical point. To our knowledge, these are the first theoretical predictions for the confinement-induced shift in the $L-L$ critical point for a ''waterlike'' model.

To further explore the effects of confinement on the thermodynamics of the associating fluid film, we examine the behavior of the mixed stress–strain expansivity $\alpha_{\parallel}$, given by Eq. (2.14). This quantity measures the response of the pore density ρ_p to changes in temperature T at constant transverse pressure $P_{\parallel}$ and pore width L. Note that $\alpha_{\parallel}$ approaches the standard coefficient of thermal expansion α_P in the limit $L\to\infty$. As is well known, bulk water exhibits negative thermal expansion ($\alpha_P<0$) over a large range of pressure P and temperature T. The region of the bulk phase diagram with $\alpha_P<0$ is enclosed by the locus of extrema in density (commonly referred to as the temperature of maximum/minimum density or the TMD). Figure 7 illustrates that negative thermal expansivity ($\alpha_{\parallel}<0$) is also a prominent feature in the confined fluid film. Interestingly, the shape and extent of the region of negative thermal expansivity (enclosed by the TMD) remains largely unchanged even for the strongly confined fluid.

The confinement-induced reduction of favorable fluid-fluid interactions does have important thermodynamic implications for the pore fluid, even at room temperature. To understand this, consider a liquid confined between hydrophobic plates with subcritical temperature T and chemical potential μ imposed on it by a reservoir. As the plates are brought close together, a separation can be reached at which point the energetic penalty of confinement causes the liquid to become metastable with respect the vapor phase.[63–67] At even closer separations, a limit of mechanical stability (i.e., a spinodal) will be reached, where the fluid in the pore spontaneously evaporates. The resulting pressure imbalance induces a long-ranged attractive interaction between the confining walls. It is believed that this solvent-induced hydrophobic interaction has implications for the stability of mesoscopic biological assemblies and protein folding.[95–99,67] A simple macroscopic scaling argument[66] predicts that the evaporation of water confined by hydrophobic walls should occur at $L\approx 100$ nm at room temperature.

To analyze the stability of the associating fluid film in the mean-field theory, we focus on the excess grand potential per unit area $\Delta\Omega_s/A$,

$$\Delta\Omega_s/A=-(P_{\parallel}-P^{\mathrm{bulk}})L, \tag{4.9}$$

where $L=\zeta d_{fw}$ for the fluid film. The quantity $\Delta\Omega_s$ in Eq. (4.9) is the difference between the grand potential of the fluid film $\Omega=-P_{\parallel}LA$, given by Eq. (2.13), and the grand potential $-P^{\mathrm{bulk}}LA$ for a region of the same size in the bulk fluid at the same temperature T and chemical potential μ. The equilibrium thermodynamic state for the film is the one for which $\Delta\Omega_s/A$ is minimum[69] consistent with its temperature T, chemical potential μ, and pore width L. Figure 8 illustrates the pore width dependence of the liquid and vapor branches of $\Delta\Omega_s/A$ for the associating fluid between hard plates [$\Psi_p(\zeta)=0$] at room temperature $T=298$ K and $\mu=-183.56$ kJ/mol. At this T and μ, the bulk fluid pressure, as determined by Eq. (3.38) in the limit $\zeta\to\infty$, is $P^{\mathrm{bulk}}=28.4$ bar. This value was selected because it is the pressure at which the boiling temperature is 373 K for the bulk associating fluid. In satisfying agreement with the simple scaling argument of Lum and Luzar,[66] Fig. 8 illustrates that the vapor is indeed the stable thermodynamic phase at separations smaller than $\zeta d_{fw}\approx 67$ nm. Also shown is the separation at which the fluid reaches a limit of mechanical stability, i.e., where $(\partial P_{\parallel}/\partial\rho)_{T,L}=0$. Consistent with previous theoretical treatments,[63,67] this ''spinodal'' is predicted to occur at nanoscale separations ($\zeta d_{fw}\approx 1$ nm). We note that hydrogen bonding is not required for the confinement-induced evaporation of a fluid,[63,100] so long as the fluid–fluid interactions are more favorable than the fluid–wall interactions. In fact, the mean-field theory presented here predicts a scenario qualitatively similar to Fig. 8 for the confined vdW fluid (not shown).

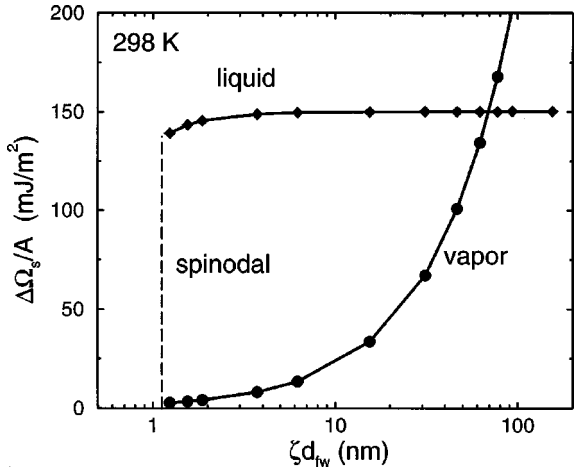

FIG. 8. The excess grand potential per unit area $\Delta\Omega_s/A$ vs dimensional pore width ζd_{fw} for the liquid (diamonds) and the vapor (circles) in the mean-field associating fluid film at $T=298$ K and $\mu=-183.56$ kJ/mol. For this case, the walls are purely repulsive ($\epsilon_{fw}=0$). The vapor is the stable thermodynamic phase for separations smaller than $\zeta d_{fw}\approx 67$ nm. The mechanical limit of stability (spinodal) for the liquid phase occurs at $\zeta d_{fw}\approx 1$ nm.

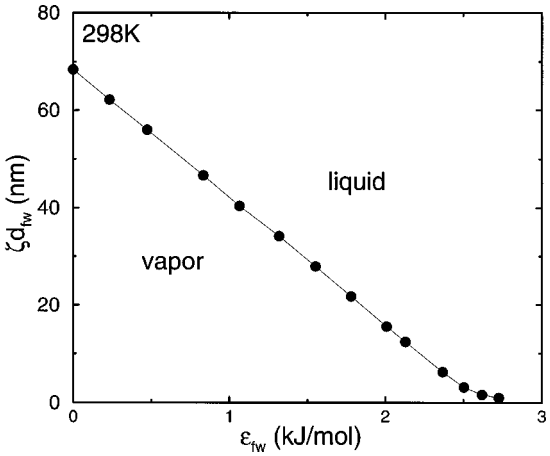

FIG. 9. The locus of liquid-vapor phase coexistence (circles) in the $\zeta d_{fw}-\epsilon_{fw}$ plane for $T=298$ K and $\mu=-183.56$ kJ/mol. The liquid phase is destabilized by reducing the pore width ζ or the magnitude of the fluid–wall attraction ϵ_{fw}.

To examine the effect of fluid–wall interactions on the thermodynamic stability of the associating fluid film, we have mapped the locus of vapor–liquid coexistence in the $\zeta d_{fw}-\epsilon_{fw}$ plane. Specifically, Fig. 9 illustrates the phase diagram for the confined fluid film for the conditions presented in Fig. 8 ($T=298$ K and $\mu=-183.56$ kJ/mol). As expected, the liquid film is destabilized with respect to evaporation at a given separation by reducing ϵ_{fw} (turning down the favorable fluid–wall interactions). Likewise, at a given ϵ_{fw}, destabilization occurs by bringing the substrates together. As can be seen, the thermodynamic driving force for confinement-induced evaporation at $T=298$ K vanishes for fluid–wall interactions that are sufficiently favorable ($\epsilon_{fw}\approx 2.75$ kJ/mol).

B. Level 2: Inhomogeneous reference fluid

In the second level of approximation, we explicitly account for the inhomogeneous structure of the confined hard-sphere reference fluid. Specifically, for a given mean number density ρ_p and pore width $\zeta=L/d_{dw}$, we determine the density profile $\rho(z)$ via the simple free energy density-functional theory (DFT) outlined in Appendix B. The details of the density profile are then utilized to determine two basic quantities in the theory: the pore probability function $p_j^{\text{pore}}(\rho_p,\zeta)$ and the excluded-volume parameter $b_p(\zeta)$. For $p_j^{\text{pore}}(\rho_p,\zeta)$, we assume that the bulk hard-sphere statistics [as described by Eq. (4.1)] apply locally, i.e., when evaluated at the local packing fraction $\eta(z)$ (see Appendix C). Hence, $p_j^{\text{pore}}(\rho_p,\zeta)$ can be written as an average over the infinitesimally thin z-directed ''layers'' in the pore,

$$p_j^{\text{pore}}(\rho_p,\zeta)\approx\frac{\int_{d_{fw}}^{s_z-d_{fw}}dz\,\rho(z)p_j^{\text{bulk}}(\eta(z))}{(s_z-2d_{fw})\rho_p},\qquad(4.10)$$

where $\rho_p=(s_z-2d_{fw})^{-1}\int_{d_{fw}}^{s_z-d_{fw}}dz\,\rho(z)$. As discussed in Sec. III, the excluded volume parameter $b_p(\zeta)$ can be evaluated explicitly using $\rho(z)$, Eq. (3.34), and Eq. (3.33). The global phase behavior for the fluid film, as described by the theory at this second of level of approximation [i.e., with the modified $p_j^{\text{pore}}(\rho_p,\zeta)$ and $b_p(\zeta)$], is examined below.

Figure 10 illustrates the $P_\parallel-T$ and $T-\rho_p$ projections of the fluid film phase diagram for varying degrees of confine-

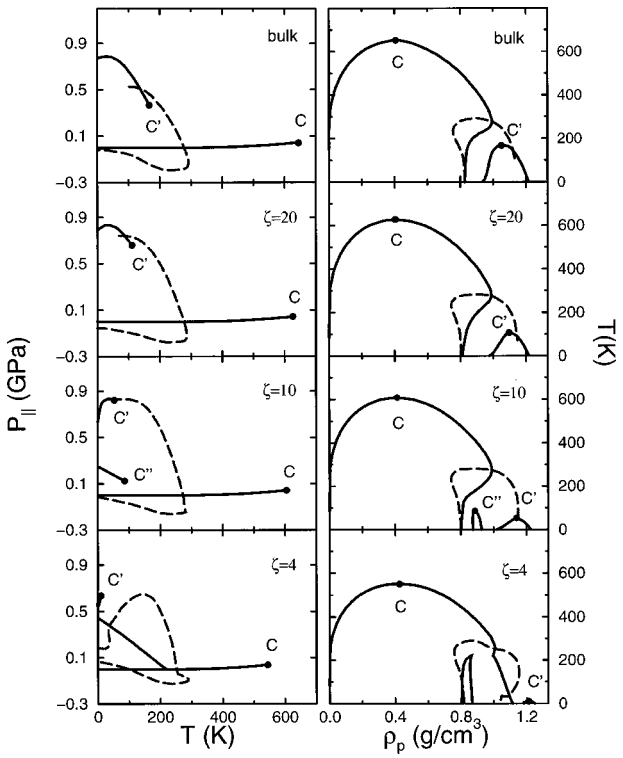

FIG. 10. Phase diagrams for the associating fluid film as determined by the second level of approximation (i.e., with the inhomogeneous reference fluid) in the $P_\parallel-T$ (left) and $T-\rho_p$ (right) planes. From bottom to top, the phase behaviors correspond to pores of dimensionless width $\zeta=4$, 10, 20, and ∞, respectively. Solid lines represent loci of phase coexistence and the dashed lines are TMDs (states with $\alpha_\parallel=0$). The liquid–vapor (C) and the liquid–liquid (C') critical points are also shown. Notice that a third fluid-fluid phase transition that terminates in a critical point (C'') appears for dimensionless pore width $\zeta=10$.

ment. Specifically, phase diagrams for dimensionless pore widths $\zeta=4$, 10, 20, and ∞ are included (corresponding to dimensional pore widths $\zeta d_{fw}\approx 1.2$ nm, 3.1 nm, 6.2 nm, and ∞, respectively). The black solid lines represent loci of phase coexistence, while the dashed lines are the loci of state points with $\alpha_{\|}=0$ (i.e., TMDs). Notice that the explicit incorporation of $\rho(z)$ for the reference fluid does very little to alter the predicted effects of confinement on the liquid–vapor $(L-V)$ transition relative to the predictions of the simple mean-field theory shown in Fig. 5. That is to say, in agreement with experimental data on a number of pore fluids,[13,15] the $L-V$ critical point is shifted to lower temperature T, lower transverse pressure $P_{\|}$, and higher pore density ρ_p.

On the other hand, the incorporation of $\rho(z)$ for the reference system dramatically affects the predictions for the low-temperature thermodynamic behavior of the strongly confined fluid. Most notably, we see the appearance of a third liquid–liquid phase transition that terminates in a critical point (C''). At a dimensionless separation $\zeta=10$, this new critical point is located at $T=86$ K, $P_{\|}=0.125$ GPa, and $\rho_p=0.886$ g/cm^3. Interestingly, as the degree of confinement increases, C'' shifts to higher temperature T, lower density ρ_p, and lower transverse pressure $P_{\|}$. In fact, at a reduced separation of $\zeta=4$, the third fluid–fluid transition has intersected the liquid–vapor transition, giving rise to a fluid–fluid–fluid triple point at $T=219$ K and $P_{\|}=4.1\times10^{-4}$ GPa.

The confinement-induced shifts in the bulk $L-V$ and $L-L$ critical points (C and C') are illustrated in Fig. 11 [the shift in the third critical point (C'') is not shown because it is absent in the bulk phase diagram]. First, we note that confinement shifts both the $L-V$ and the $L-L$ critical points to lower temperature T and higher pore density ρ_p. Moreover, as predicted by the mean-field theory, we see that the shift in the $L-V$ critical point for the associating fluid tracks very closely the shift for the vdW fluid film. However, in contrast to the mean-field predictions, the dependence of the critical transverse pressure $P_{\|,C}$ for the $L-L$ transition is appreciably nonmonotonic, exhibiting a maximum at $\zeta\approx 10$.

The predictions of the theory at this level are especially interesting in light of two recent computer simulation studies on the behavior of supercooled ''waterlike'' models confined between hydrophobic walls. In the first, Koga *et al.*[56] searched for signatures of the a low-temperature liquid–liquid phase transition in a film of TIP4P water[101] confined between walls that interact with the fluid via a 9-3 potential. The TIP4P model for water was chosen because, under certain pressure conditions (e.g., $P^{\text{bulk}}=1\times10^{-4}$ GPa), the bulk fluid is reported to exhibit pronounced discontinuities in density and energy[47,102] at low temperature, indicative of a polyamorphic phase transition. However, in their molecular dynamics simulations (at fixed N, P_{zz}, and T) of a film of thickness $\zeta d_{fw}\approx 2$ nm, no signatures of the transition were detected at either $P_{zz}=1\times10^{-4}$ GPa or $P_{zz}=0.5$ GPa. The plausible conclusion drawn by the authors was that confinement had dramatically shifted the location liquid–liquid immiscibility to lower temperature.

In the second study of interest, Meyer and Stanley[68] investigated the behavior of a film of ST2 water[103] confined between hydrophobic walls that similarly interacted with the fluid via a 9-3 Lennard-Jones potential. However, unlike in the investigation of Koga *et al.*,[56] their Monte Carlo simulations (at fixed N, ρ_p, and T) revealed strong signatures of the

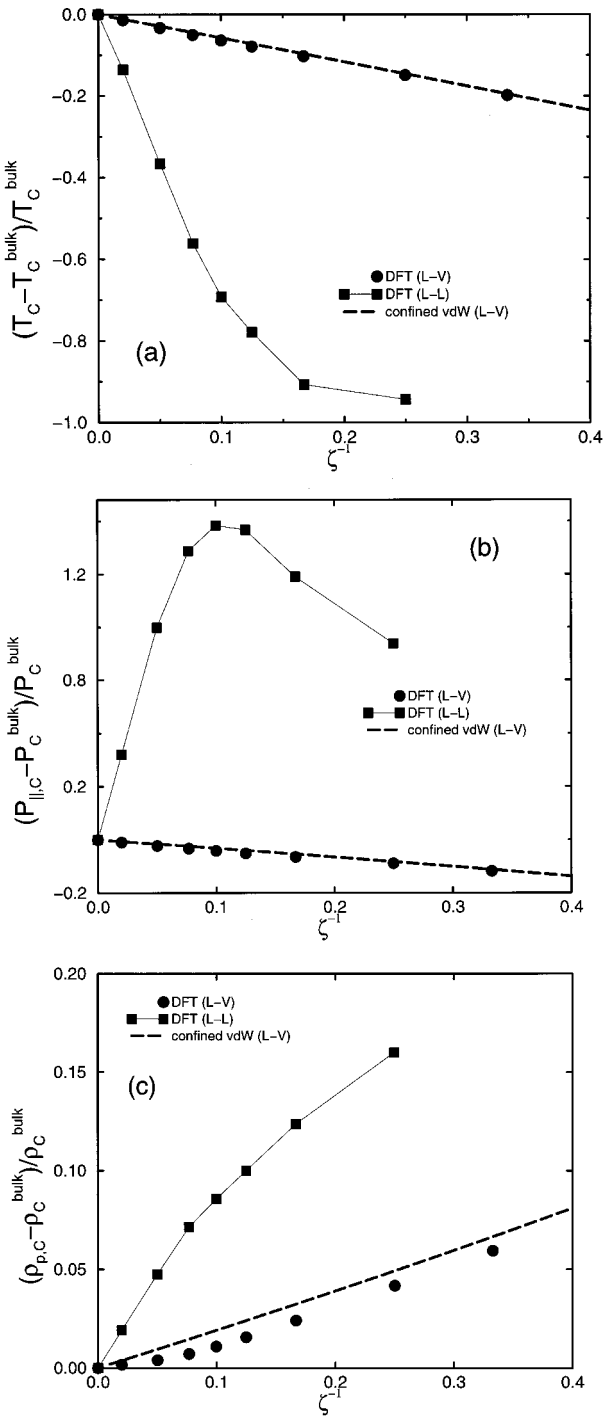

FIG. 11. Relative shifts for the liquid–vapor $(L-V)$ and the liquid–liquid $(L-L)$ critical points in the fluid film versus inverse pore width ζ^{-1} as determined by the second level of approximation (i.e., with the inhomogeneous reference fluid): (a) $(T_c-T_c^{\text{bulk}})/T_c^{\text{bulk}}$, (b) $(P_{\|,c}-P_c^{\text{bulk}})/P_c^{\text{bulk}}$, and (c) $(\rho_{p,c}-\rho_c^{\text{bulk}})/\rho_c^{\text{bulk}}$. Shown are results for the $L-V$ transition in the confined vdW fluid (dashed line) and the mean-field associating fluid (black circles). The relative shift for the $L-L$ transition in the associating fluid film (black squares) is also illustrated. The third fluid–fluid critical point discussed in the text is not shown since it does not appear in the bulk.

second phase transition for a film thickness of $\zeta d_{fw} \approx 1$ nm. These signatures, however, were detected at much lower pore density and transverse pressure ($\rho_p \approx 0.8\ \mathrm{g/cm^3}$ and $P_\parallel \approx 0.05$ GPa) than those estimated for C' in the bulk ST2 fluid ($\rho_p \approx 0.98\ \mathrm{g/cm^3}$ and $P_\parallel \approx 0.2$ GPa).[104] This indicates one of two possible conclusions: either (1) the liquid–liquid critical point (C') is shifted dramatically by confinement and/or (2) the observed signatures indicate the presence of a different phase transition.

Both of these simulation results seem to be consistent with the qualitative evolution of the phase diagram under confinement shown in Fig. 10. Namely, as concluded by Koga *et al.*,[56] the temperature of the second critical point C' is predicted to be dramatically reduced as the fluid becomes strongly confined. Moreover, we see that the theory does predict the emergence of a new phase transition at lower ρ_p and $P_\parallel$ that could (at least in principle) give rise to signatures similar to those observed by Meyer and Stanley.[68] Thus, although the approximate theory presented here is extremely simple, it provides some interesting explanations for the behavior of two water models as observed in simulations under conditions of confinement and supercooling.

V. CONCLUSIONS

A basic perturbation theory has been introduced for investigating the thermodynamics and global phase behavior of a ''waterlike'' fluid film confined between hydrophobic walls. The theory has been solved using two different levels of approximation for the confined hard-sphere reference fluid. The first level amounts to a mean-field theory that assumes the reference pore phase to be homogeneous. In the second level of the theory, a free energy density functional theory is employed to account for the inhomogeneous structure of the reference fluid.

The two levels of approximation address two physically-intuitive confinement effects. The first effect can be summarized as follows: the introduction of hydrophobic confining walls reduces the average number of favorable fluid–fluid interactions per molecule, i.e., it disrupts the hydrogen-bonding pattern in the fluid. The energetic penalty associated with this disruption, which is captured qualitatively by the theory at the mean-field level, causes the liquid–liquid critical point to shift to lower temperature, higher density, and higher pressure as the degree of confinement is increased. As is well known,[62–67] the reduction of favorable fluid–fluid interactions can also promote strong hydrophobic interactions between the confining walls at nanometer length scales, induced by the evaporation of the intervening fluid film. The mean-field theory offers a simple means for investigating the thermodynamic stability of a ''waterlike'' fluid film as a function of wall separation and the strength of the fluid–wall interaction.

The second confinement effect is the introduction of density modulations (structural inhomogeneity) into the fluid film. These density modulations (accounted for in an approximate way in the second level of the theory) can promote or disrupt hydrogen bonding in distinct ''layers,'' modifying the dependence of the hydrogen-bonding energy on the average pore density. When the density modulations are incorporated into the perturbation theory, a third fluid–fluid transition emerges in the strongly confined fluid. The appearance of this third phase transition is intriguing, especially when considered in light of recent computer simulation results of waterlike fluids confined between hydrophobic walls.[56,68]

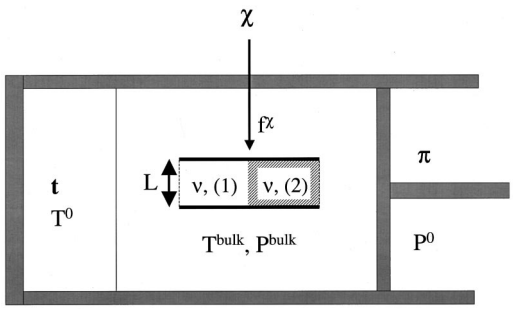

FIG. 12. Isolated composite system used in the derivation of the equilibrium criteria.

ACKNOWLEDGMENTS

We thank T. K. Vanderlick for useful discussions concerning the density functional theory of hard spheres in confinement. P.G.D. gratefully acknowledges support of the U.S. Department of Energy, Division of Chemical Sciences, Office of Basic Energy Sciences (Grant No. DE-FG02-87ER13714). S.T. was supported by the Engineering Research Program of the Office of Basic Energy Sciences at the U.S. Department of Energy (Grant No. DE-FG02-92ER14275). T.M.T. acknowledges the support of The National Science Foundation.

APPENDIX A: THE THERMODYNAMIC CRITERIA FOR EQUILIBRIUM OF COEXISTING PHASES IN THIN-FILM CONFINEMENT

Diestler and Schoen[69] have presented a lucid discussion of the thermodynamic criteria for equilibrium of a single fluid phase confined to a thin film between parallel walls. Here, we develop the analogous equilibrium criteria for single-component coexisting fluid phases {(1), (2)} in thin-film confinement.

From a thermodynamic perspective, it is convenient[69] to focus on a composite system that contains *both* the confined film (ν) [with coexisting phases (1) and (2)] and the bulk fluid (see Fig. 12). We let this composite system be in contact with three reservoirs. One of them, a thermal reservoir (t) with temperature T^0, performs no work, and interacts with the composite system through a rigid and impermeable boundary. A second reservoir (π) with pressure P^0 is purely mechanical; i.e., it can undergo only adiabatic work interactions with the composite system through an adiabatic and impermeable boundary. The final reservoir (χ) is also mechanical in nature, providing uniform load per unit area f^χ to the confining walls which can be used to manipulate their separation L. Note that the system depicted in Fig. 12 provides no mechanical coupling to the surroundings by means of which the total area $A = A^{(1)} + A^{(2)}$ of the fluid film in

contact with a confining wall can be varied. However, the individual contributions to the fluid–wall area from coexisting phases [$A^{(1)}$ and $A^{(2)}$] can clearly be simultaneously varied within this ''fixed area'' constraint.

We take the confined film, the bulk fluid, and the reservoirs to constitute an isolated composite system. At equilibrium, the energy of this isolated system is a minimum consistent with its entropy. In other words, virtual transformations that would remove the system from the equilibrium state must satisfy

$$\delta(U^{\text{bulk}}+U^{\nu,(1)}+U^{\nu,(2)}+U^{t}+U^{\pi}+U^{\chi})\geqslant 0 \tag{A1}$$

subject to the constraint

$$\delta(S^{\text{bulk}}+S^{\nu,(1)}+S^{\nu,(2)}+S^{t})=0. \tag{A2}$$

Note that since the mechanical reservoirs (π and χ) interact adiabatically with the composite system, we have

$$\delta S^{\pi}=\delta S^{\chi}=0. \tag{A3}$$

The fundamental equation relating changes in the internal energy of the bulk fluid to infinitesimal and reversible variations in the corresponding independent variables is

$$\delta U^{\text{bulk}}=T^{\text{bulk}}\delta S^{\text{bulk}}-P^{\text{bulk}}\delta V^{\text{bulk}}+\mu^{\text{bulk}}\delta N^{\text{bulk}}. \tag{A4}$$

A similar relationship applies in the confined phases,[69]

$$\delta U^{\nu,(k)}=T^{\nu,(k)}\delta S^{\nu,(k)}-P_{\parallel}^{\nu,(k)}L\,\delta A^{(k)}-P_{zz}^{\nu,(k)}A^{(k)}\delta L+\mu^{\nu,(k)}\delta N^{\nu,(k)}. \tag{A5}$$

Here, k identifies the phase ($k=1,2$), $U^{\nu,(k)}$ represents the internal energy, $T^{\nu,(k)}$ is the temperature, $S^{\nu,(k)}$ is the entropy, $\mu^{\nu,(k)}$ is the chemical potential, $N^{\nu,(k)}$ is the number of molecules, and $P_{\parallel}^{\nu,(k)}$ and $P_{zz}^{\nu,(k)}$ represent the transverse and normal components of the pressure tensor, respectively. For the reservoirs, we have

$$\delta U^{\chi}=f^{\chi}A\,\delta L, \tag{A6}$$

$$\delta U^{t}=T^{0}\delta S^{t}, \tag{A7}$$

and

$$\delta U^{\pi}=-P^{0}\delta V^{\pi}. \tag{A8}$$

Moreover, since the composite system is isolated, we have the following additional constraints,

$$\delta V^{\pi}+\delta V^{\nu,(1)}+\delta V^{\nu,(2)}+\delta V^{\text{bulk}}=0 \tag{A9}$$

and

$$\delta N^{\nu,(1)}+\delta N^{\nu,(2)}+\delta N^{\text{bulk}}=0. \tag{A10}$$

Combining Eqs. (A1)–(A10), we obtain

$$(T^{\text{bulk}}-T^{0})\delta S^{\text{bulk}}+(T^{\nu,(1)}-T^{0})\delta S^{\nu,(1)}+(T^{\nu,(2)}-T^{0})\delta S^{\nu,(2)}-(P^{\text{bulk}}-P^{0})\delta V^{\text{bulk}}-(P_{zz}^{\nu,(1)}A^{(1)}+P_{zz}^{\nu,(2)}A^{(2)}-f^{\chi}A-P^{0}A)\delta L-(P_{\parallel}^{\nu,(1)}-P_{\parallel}^{\nu,(2)})L\,\delta A^{(1)}+(\mu^{\nu,(1)}-\mu^{\text{bulk}})\delta N^{\nu,(1)}+(\mu^{\nu,(2)}-\mu^{\text{bulk}})\delta N^{\nu,(2)}\geqslant 0. \tag{A11}$$

Because we require the equality in Eq. (A11) to hold at equilibrium for independent variations in S^{bulk}, $S^{\nu,(1)}$, $S^{\nu,(2)}$, V^{bulk}, L, $A^{(1)}$, $N^{\nu,(1)}$, and $N^{\nu,(2)}$, the equilibrium conditions are as follows:

$$\begin{aligned}
&T^{\text{bulk}}=T^{\nu,(1)}=T^{\nu,(2)}=T^{0},\\
&\mu^{\text{bulk}}=\mu^{\nu,(1)}=\mu^{\nu,(2)},\\
&P^{\text{bulk}}=P^{0},\\
&P_{zz}^{\nu,(1)}=P_{zz}^{\nu,(2)},\\
&P_{zz}^{\nu,(1)}=f^{\chi}+P^{0},\\
&P_{\parallel}^{\nu,(1)}=P_{\parallel}^{\nu,(2)}.
\end{aligned} \tag{A12}$$

Note that the equality $P_{zz}^{\nu,(1)}=P_{zz}^{\nu,(2)}$ is required for mechanical equilibrium of the parallel plates. If we do not allow for the possibility of variations in the film thickness (i.e., $\delta L=0$), then the equilibrium conditions reduce to the following:

$$\begin{aligned}
&T^{\text{bulk}}=T^{\nu,(1)}=T^{\nu,(2)}=T^{0},\\
&\mu^{\text{bulk}}=\mu^{\nu,(1)}=\mu^{\nu,(2)},\\
&P^{\text{bulk}}=P^{0},\\
&P_{\parallel}^{\nu,(1)}=P_{\parallel}^{\nu,(2)},
\end{aligned} \tag{A13}$$

indicating that coexistence requires equality of temperature, chemical potential, and transverse pressure between the phases.

APPENDIX B: DENSITY FUNCTIONAL THEORY FOR THE INHOMOGENEOUS REFERENCE FLUID

The inhomogeneous reference fluid discussed in Secs. III and IV is simply a collection of identical hard spheres with diameter d_f whose centers are confined by parallel hard walls to a slit of width $L=\zeta d_{fw}$. A natural and well-known strategy for determining the density profile of this system is to employ a free energy density functional theory (DFT).[105–107] In short, a free energy DFT involves the construction of an expression that relates the Helmholtz free energy of the system F to the density profile $\rho(\mathbf{r})$. The equilibrium density profile, consistent with the proposed free energy functional, is that profile which minimizes the free energy F subject to conservation of the particles. Equivalently, the density profile is an unconstrained minimum of the grand potential Ω, where

$$\Omega=F-\mu\int\rho(\mathbf{r})d\mathbf{r}. \tag{B1}$$

Hence, the equilibrium density profile is a solution to the following Euler–Lagrange equation for the minimization of Ω,

$$\mu=\frac{\delta F}{\delta\rho(\mathbf{r})}. \tag{B2}$$

For a system of hard spheres, F can be decomposed into three contributions,

$$F=F^{\text{ext}}+F^{\text{ideal}}+F^{\text{excess}}, \tag{B3}$$

which represent the external field (e.g., confining walls), the ideal gas, and the excess due to the hard-sphere interaction, respectively. The contributions from the external field F^{ext} and the ideal gas F^{ideal} are given by

$$F^{\text{ext}} = \int \rho(\mathbf{r}) u^{\text{ext}}(\mathbf{r}) d\mathbf{r} \tag{B4}$$

and

$$F^{\text{ideal}} = N\mu^*(T) + k_B T \int \rho(\mathbf{r})[\ln \rho(\mathbf{r}) - 1] d\mathbf{r}, \tag{B5}$$

where $u^{\text{ext}}(\mathbf{r})$ is the external potential acting on the spheres, k_B is Boltzmann's constant, and $\mu^*(T)$ accounts for the internal degrees of freedom of the ideal gas molecules.

Percus has developed[108] the following generic free energy functional for the excess contribution F^{excess} based on exact one-dimensional results,[109]

$$F^{\text{excess}} = \int \overline{\rho}^{\mathcal{Z}}(\mathbf{r}) \mathcal{F}_0[\overline{\rho}^{\mathcal{Y}}(\mathbf{r})] d\mathbf{r}, \tag{B6}$$

where $\mathcal{F}_0(\rho)$ is the excess free energy per particle for the uniform fluid with number density ρ and the pair $\overline{\rho}^{\mathcal{Z}}(\mathbf{r})$ and $\overline{\rho}^{\mathcal{Y}}(\mathbf{r})$ represent the following weighted coarse-grained densities:

$$\begin{aligned} \overline{\rho}^{\mathcal{Z}}(\mathbf{r}) &= \int \mathcal{Z}(\mathbf{r}-\mathbf{r}')\rho(\mathbf{r}') d\mathbf{r}', \\ \overline{\rho}^{\mathcal{Y}}(\mathbf{r}) &= \int \mathcal{Y}(\mathbf{r}-\mathbf{r}')\rho(\mathbf{r}') d\mathbf{r}'. \end{aligned} \tag{B7}$$

The kernels $\mathcal{Z}$ and $\mathcal{Y}$ are local weighting functions to be prescribed. The chemical potential, according to Eq. (B2), is related to the density profile through

$$\begin{aligned} R[\rho(z),z] = 0 = &-\mu + u^{\text{ext}}(\mathbf{r}) + k_B T \ln \rho(\mathbf{r}) \\ &+ \int \frac{\delta \overline{\rho}^{\mathcal{Z}}(\mathbf{r}')}{\delta \rho(\mathbf{r})} \mathcal{F}_0[\overline{\rho}^{\mathcal{Y}}(\mathbf{r}')] d\mathbf{r}' \\ &+ \int \frac{\delta \overline{\rho}^{\mathcal{Y}}(\mathbf{r}')}{\delta \rho(\mathbf{r})} \overline{\rho}^{\mathcal{Z}}(\mathbf{r}') \mathcal{F}_0'[\overline{\rho}^{\mathcal{Y}}(\mathbf{r}')] d\mathbf{r}', \end{aligned} \tag{B8}$$

where $\mathcal{F}_0'(\rho)$ is the derivative of $\mathcal{F}_0(\rho)$ with respect to density. The right-hand side of Eq. (B8) defines a functional residual $R[\rho(z);z]$ which, for the equilibrium density profile, must satisfy $R[\rho(z);z] = 0$ for all z.

To complete the theory, a precise form must be prescribed for the weighting functions ($\mathcal{Z}$ and $\mathcal{Y}$) and the excess free energy per particle for the uniform hard-sphere fluid $\mathcal{F}_0(\rho)$. Then, for a given external potential $u^{\text{ext}}(\mathbf{r})$ and chemical potential μ, the equilibrium density profile is obtained by solving Eq. (B8).

For a system of hard spheres of diameter d_f whose centers are confined to z-coordinates $-\zeta d_{fw}/2 < z < \zeta d_{fw}/2$, the total external potential is given by

$$u^{\text{ext}}(z) = u_{\text{wall}}\left(\frac{\zeta d_{fw}}{2} - z\right) + u_{\text{wall}}\left(\frac{\zeta d_w}{2} + z\right), \tag{B9}$$

where

$$u_{\text{wall}}(r) = \begin{cases} 0 & r > 0 \\ \infty & r \leqslant 0 \end{cases}. \tag{B10}$$

In this study we employ the generalized hard-rod model[110,111] for F^{excess}, which requires

$$\mathcal{Z}(z) = d_f^{-1} \Theta\left(\frac{d_f}{2} - |z|\right) \tag{B11}$$

and

$$\mathcal{Y}(z) = \frac{6}{d_f^3} \Theta\left(\frac{d_f}{2} - |z|\right)\left[\left(\frac{d_f}{2}\right)^2 - z^2\right], \tag{B12}$$

where Θ is the Heaviside step function. For the uniform free energy per particle $\mathcal{F}_0$, we use the familiar Carnahan–Starling[112] expression,

$$\mathcal{F}_0\left(\eta = \frac{\pi d_f^3 \rho}{6}\right) = k_B T \frac{\eta(4-3\eta)}{(1-\eta)^2}. \tag{B13}$$

To obtain the equilibrium density profile, the integral relation (B8) was solved numerically subject to Eqs. (B7), (B9), (B10), (B11), (B12), and (B13). In this study, Eq. (B8) was discretized uniformly with mesh size $0.02 d_f$ over the domain of interest $-\zeta d_{fw}/2 < z < \zeta d_{fw}/2$, and all integrals were evaluated via the trapezoidal rule. This generates a set of nonlinear coupled algebraic equations for the nodal densities that is conveniently solved by Newton iteration.[107] The details of this numerical technique are outlined elsewhere.[107,113]

Although the natural input variables to the density functional calculation are the chemical potential μ of the confined hard-sphere fluid and the pore width ζd_{fw}, it is more convenient for our purposes to input the mean pore density ρ_p and the pore width ζd_{fw}. This change of input variables is easily accommodated[113] by augmenting the set of nonlinear equations for the nodal densities with a residual equation for the specified pore density ρ_p. The corresponding additional ''unknown'' is the chemical potential μ.

APPENDIX C: PACKING IN THE SLIT-PORE GEOMETRY

Consider a collection of hard spheres of diameter d_f whose centers are confined by hard walls to a slit of width $L = s_z - 2d_{fw} = \zeta d_{fw}$. The spatial distribution of particle centers inside of this slit-pore geometry will generally be nonuniform in the z-direction (i.e., the direction normal to the walls). In particular, the number of particle centers $dN(z)$ that are contained in the infinitesimally thin rectangular region of volume Adz centered at z is determined by the number density profile $\rho(z)$,

$$dN(z) = \rho(z) A dz. \tag{C1}$$

It follows that the average number density ρ_p in the pore is given by

$$\rho_p = (s_z - 2d_{fw})^{-1} \int_{d_{fw}}^{s_z - d_{fw}} dz \rho(z) = N/[A(s_z - 2d_{fw})]. \tag{C2}$$

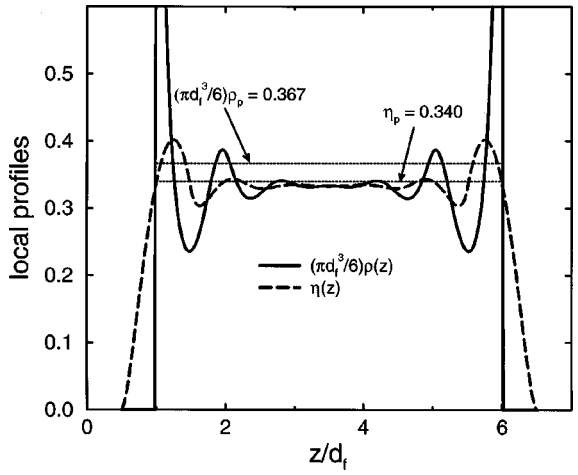

FIG. 13. Density profile $\rho(z)$ (solid), packing fraction profile $\eta(z)$ (long-dashed), and mean packing fraction η_p (dotted) for a confined hard-sphere fluid at $\rho_p=0.70$ as calculated by the density functional theory outlined in Appendix B.

In a similar fashion, the nonuniform spatial distribution of the local packing fraction in the slit-pore geometry can be described by a packing profile $\eta(z)$. The quantity $\eta(z)$ is simply the probability that a randomly chosen point on the plane of area A centered at z lies within a distance $d_f/2$ of a sphere center. Note that because the sphere centers can access the region $d_{fw}<z<s_z-d_{fw}$, the sphere volumes can intersect $x-y$ planes centered at z in the range $d_w/2<z<s_z-d_w/2$.

The local packing fraction $\eta(z)$ can be determined by integrating over the area of intersection $A^{\mathrm{int}}(z,z')$ between each sphere centered at z' and the plane at z,

$$\eta(z)=\int_{z-d_f/2}^{z+d_f/2}dz'\rho(z')A^{\mathrm{int}}(z,z')$$
$$=\int_{z-d_f/2}^{z+d_f/2}dz'\rho(z')\pi\left[\left(\frac{d_f}{2}\right)^2-(z-z')^2\right]. \quad \text{(C3)}$$

Furthermore, integrating Eq. (C3) from ''wall to wall'' must yield, as a normalization condition, the total volume of the spheres divided by the cross-sectional area A,

$$\int_{d_w/2}^{s_z-d_w/2}dz'\,\eta(z')=\frac{\pi d_f^3 N}{6A}=\frac{\pi d_f^3\rho_p}{6}(s_z-2d_{fw}), \quad \text{(C4)}$$

where the last equality follows from Eq. (C2). We are interested in calculating the average packing fraction η_p for the thermodynamic system, i.e., for the volume $A(s_z-2d_{fw})$ accessible to the sphere centers,

$$\eta_p=(s_z-2d_{fw})^{-1}\int_{d_{fw}}^{s_z-d_{fw}}dz\,\eta(z)$$
$$=\frac{\pi d_f^3\rho_p}{6}-\frac{2}{s_z-2d_{fw}}\int_{d_w/2}^{d_{fw}}dz\,\eta(z). \quad \text{(C5)}$$

Figure 13 illustrates $\rho(z)$, $\eta(z)$, and η_p for a confined hard-sphere fluid at $\rho_p=0.70$ as calculated by the density functional theory outlined in Appendix B. Note that $\rho(z)=0$ for $z<d_{fw}$ and $z>s_z-d_{fw}$, while $\eta(z)\neq 0$ in this region.

Substituting Eq. (C3) into Eq. (C5) and using the fact that $\rho(z)=0$ for $z<d_{fw}$ yields the following exact relationship between the density profile $\rho(z)$ and the average packing fraction η_p:

$$\eta_p=\frac{\pi d_f^3\rho_p}{6}-\frac{2}{s_z-2d_{fw}}\int_{d_w/2}^{d_{fw}}dz\int_{d_{fw}}^{z+d_f/2}dz'\rho(z')\pi$$
$$\times\left[\left(\frac{d_f}{2}\right)^2-(z-z')^2\right]. \quad \text{(C6)}$$

Of course, in the limit $s_z\to\infty$, we recover the bulk relationship between the packing fraction η and the number density ρ,

$$\eta=\frac{\pi d_f^3\rho}{6}. \quad \text{(C7)}$$

Moreover, for a uniform density profile in the slit pore [i.e., $\rho(z)=\rho_p$ for $d_{fw}<z<s_z-d_{fw}$], we have

$$\eta_p=\frac{\pi d_f^3\rho_p}{6}\left[1-\frac{3}{16\zeta}\right]. \quad \text{(C8)}$$

This relationship is employed in the mean-field theory outlined in Sec. IV.

[1] R. M. Barrer, *Zeolites and Clay Minerals as Sorbents and Molecular Sieves* (Academic, London, 1978).
[2] E. Roedder, Rev. Mineral. **12**, 1 (1984).
[3] H. E. Warriner, S. H. J. Idziak, N. L. Slack, P. Davidson, and C. R. Safinya, Science **271**, 969 (1996).
[4] B. M. Discher *et al.*, Science **284**, 1143 (1999).
[5] *Structure and Dynamics of Membranes*, Vols. 1A and 1B, in *Handbook of Biological Physics*, edited by R. Lipowsky and E. Sackmann (Elsevier, Amsterdam, 1995).
[6] B. Hille, *Ionic Channels of Excitable Membranes* (Sinauer, Sunderland, MA, 1992).
[7] P. Jenniskens, D. F. Blake, M. A. Wilson, and A. Pohorille, Astrophys. J. **455**, 389 (1995).
[8] J. Dore, *Correlations and Connectivity*, edited by H. E. Stanley and N. Ostrowsky (Kluwer Academic, Dordrecht, 1990), p. 188.
[9] P. G. Debenedetti, *Metastable Liquids*: *Concepts and Principles* (Princeton University Press, Princeton, 1996).
[10] S.-H. Chen and M.-C. Bellissent-Funel, *Hydrogen Bond Networks*, NATO ASI Series C: Mathematical and Physical Science, edited by M.-C. Bellissent-Funel and J. C. Dore (Kluwer Academic, Dordrecht, 1994), Vol. 435, p. 307.
[11] M.-C. Bellissent-Funel, J. Mol. Liq. **78**, 19 (1998).
[12] M. Freemantle, Chem. Eng. News **77**, 27 (1999).
[13] R. Evans, J. Phys.: Condens. Matter **2**, 8989 (1990).
[14] B. J. Frisken, A. J. Liu, and D. S. Cannell, Mater. Res. Bull. **29**, 19 (1994).
[15] L. D. Gelb, K. E. Gubbins, R. Radhakrishnan, and M. Sliwinska-Bartkowiak, Rep. Prog. Phys. **62**, 1573 (1999).
[16] Y. B. Melnichenko, J. Schüller, R. Richert, B. Ewen, and C. K. Loong, J. Chem. Phys. **103**, 2016 (1995).
[17] M. Arndt, R. Stannarius, H. Groothues, E. Hempel, and F. Kremer, Phys. Rev. Lett. **79**, 2077 (1997).
[18] G. Barut, P. Pissis, R. Pelster, and G. Nimtz, Phys. Rev. Lett. **80**, 3543 (1998).
[19] J.-Y. Park and G. B. McKenna, Phys. Rev. B **61**, 6667 (2000).
[20] P. Gallo, Phys. Chem. Chem. Phys. **2**, 1607 (2000).
[21] D. E. Hare and C. M. Sorensen, J. Chem. Phys. **87**, 4840 (1987).
[22] D. Eisenberg and W. Kauzmann, *The Structure and Properties of Water* (Oxford University Press, New York, 1969).
[23] F. H. Stillinger and P. G. Debenedetti, J. Phys. Chem. B **103**, 4052 (1999).
[24] R. J. Speedy and C. A. Angell, J. Chem. Phys. **65**, 851 (1976).
[25] C. A. Angell, M. Oguni, and W. J. Sichina, J. Phys. Chem. **86**, 998 (1982).
[26] E. Tombari, C. Ferrari, and G. Salvetti, Chem. Phys. Lett. **300**, 749 (1999).

[27] C. A. Angell, E. D. Finch, L. A. Woolf, and P. Bach, J. Chem. Phys. **65**, 3063 (1976).
[28] F. X. Prielmeier, E. W. Lang, R. J. Speedy, and H.-D. Lüdemann, Phys. Rev. Lett. **59**, 1128 (1987).
[29] P. V. Hobbs, *Ice Physics* (Clarendon, Oxford, 1974).
[30] C. Lobban, J. L. Finney, and W. F. Kuhs, J. Chem. Phys. **112**, 7169 (2000).
[31] O. Mishima, L. D. Calvert, and E. Whalley, Nature (London) **314**, 76 (1985).
[32] O. Mishima, J. Chem. Phys. **100**, 5910 (1994).
[33] P. H. Poole, T. Grande, F. Sciortino, H. E. Stanley, and C. A. Angell, Comput. Mater. Sci. **4**, 373 (1995).
[34] M.-C. Bellissent-Funel, Europhys. Lett. **42**, 161 (1998).
[35] G. P. Johari, J. Chem. Phys. **105**, 7079 (1996).
[36] R. J. Speedy, P. G. Debenedetti, R. S. Smith, C. Huang, and B. D. Kay, J. Chem. Phys. **105**, 240 (1996).
[37] H. E. Stanley and J. Teixeira, J. Chem. Phys. **73**, 3404 (1980).
[38] Y. Xie, K. F. Ludwig, G. Morales, D. E. Hare, and C. M. Sorensen, Phys. Rev. Lett. **71**, 2050 (1993).
[39] S. Sastry, P. G. Debenedetti, F. Sciortino, and H. E. Stanley, Phys. Rev. E **53**, 6144 (1996).
[40] L.-P. Rebelo, P. G. Debenedetti, and S. Sastry, J. Chem. Phys. **109**, 626 (1998).
[41] H. Tanaka, Phys. Rev. Lett. **80**, 5750 (1998).
[42] T. M. Truskett, P. G. Debenedetti, S. Sastry, and S. Torquato, J. Chem. Phys. **111**, 2647 (1999).
[43] O. Mishima and H. E. Stanley, Nature (London) **392**, 164 (1998).
[44] O. Mishima, Phys. Rev. Lett. **85**, 334 (2000).
[45] P. H. Poole, F. Sciortino, U. Essmann, and H. E. Stanley, Nature (London) **360**, 324 (1992).
[46] S. H. Harrington, R. Zhang, P. H. Poole, F. Sciortino, and H. E. Stanley, Phys. Rev. Lett. **78**, 2409 (1997).
[47] H. A. Tanaka, Nature (London) **380**, 328 (1996).
[48] C. J. Roberts and P. G. Debenedetti, J. Chem. Phys. **105**, 658 (1996).
[49] C. J. Roberts, A. Z. Panagiotopoulos, and P. G. Debenedetti, Phys. Rev. Lett. **77**, 4386 (1996).
[50] M. R. Sadr-Lahijany, A. Scala, S. V. Buldyrev, and H. E. Stanley, Phys. Rev. Lett. **81**, 4895 (1998).
[51] E. A. Jagla, J. Chem. Phys. **111**, 8980 (1999).
[52] F. Bruni, M. A. Ricci, and A. K. Soper, J. Chem. Phys. **109**, 1478 (1998).
[53] A. K. Soper, F. Bruni, and M. A. Ricci, J. Chem. Phys. **109**, 1486 (1998).
[54] M. A. Ricci, F. Bruni, P. Gallo, M. Rovere, and A. K. Soper, J. Phys.: Condens. Matter **12**, A345 (2000).
[55] M.-C. Bellissent-Funel, R. Sridi-Dorbez, and L. Bosio, J. Chem. Phys. **104**, 10023 (1996).
[56] K. Koga, X. C. Zeng, and H. Tanaka, Chem. Phys. Lett. **285**, 278 (1998).
[57] I. Brovchenko, D. Paschek, and A. Geiger, J. Chem. Phys. **113**, 5026 (2000).
[58] R. Bergman and J. Swenson, Nature (London) **403**, 283 (2000).
[59] R. Bergman, J. Swenson, L. Börjesson, and P. Jacobsson, J. Chem. Phys. **113**, 357 (2000).
[60] G. Sartor, A. Hallbrucker, and E. Mayer, Biophys. J. **69**, 2679 (1995).
[61] M. Schoen and D. J. Diestler, J. Chem. Phys. **109**, 5596 (1998).
[62] F. H. Stillinger, J. Solution Chem. **2**, 141 (1973).
[63] D. R. Bérard, P. Attard, and G. N. Patey, J. Chem. Phys. **98**, 7236 (1993).
[64] G. Gompper, M. Hauser, and A. A. Kornyshev, J. Chem. Phys. **101**, 3378 (1994).
[65] J. Forsman, B. Jönsson, C. E. Woodward, and H. Wennerström, J. Phys. Chem. **101**, 4253 (1997).
[66] K. Lum and A. Luzar, Phys. Rev. E **56**, R6283 (1997).
[67] K. Lum, D. Chandler, and J. D. Weeks, J. Phys. Chem. B **103**, 4570 (1999).
[68] M. Meyer and H. E. Stanley, J. Phys. Chem. B **103**, 9728 (1999).
[69] D. J. Diestler and M. Schoen, Acta Chim. Hung. **132**, 45 (1995).
[70] D. J. Diestler, M. Schoen, J. E. Curry, and J. H. Cushman, J. Chem. Phys. **100**, 9140 (1994).
[71] M. Schoen, Physica A **270**, 353 (1999).
[72] D. Chandler, J. D. Weeks, and H. C. Andersen, Science **220**, 787 (1983).
[73] *Handbook of Mathematical Functions*, National Bureau of Standards, Applied Mathematical Series 55, edited by M. Abramowitz and I. R. Stegun (U.S. Government Printing Office, Washington, D.C., 1965).
[74] T. L. Hill, *Statistical Mechanics*: *Principles and Selected Applications* (Dover, New York, 1987).
[75] A. Papoulis, *Probability, Random Variables, and Stochastic Processes* (McGraw–Hill, New York, 1984).
[76] F. H. Stillinger, Science **209**, 451 (1980).
[77] J. R. Errington and P. G. Debenedetti, Nature (in press).
[78] Anonymous, Nature (London) **239**, 488 (1972).
[79] H. Reiss, H. L. Frisch, and J. L. Lebowitz, J. Chem. Phys. **31**, 369 (1959).
[80] H. Reiss and A. D. Hammerich, J. Phys. Chem. **90**, 6252 (1986).
[81] R. J. Speedy, J. Phys. Chem. **92**, 2016 (1988).
[82] H. Reiss, J. Phys. Chem. **96**, 4736 (1992).
[83] S. Torquato, Phys. Rev. E **51**, 3170 (1995).
[84] S. Torquato, Phys. Rev. Lett. **74**, 2156 (1995).
[85] T. M. Truskett, S. Torquato, and P. G. Debenedetti, Phys. Rev. E **58**, 7369 (1998).
[86] M. Thommes and G. H. Findenegg, Langmuir **10**, 4270 (1994).
[87] M. Thommes, G. H. Findenegg, and M. Schoen, Langmuir **11**, 2137 (1995).
[88] G. V. Burgess, D. H. Everett, and S. Nutall, Pure Appl. Chem. **61**, 1845 (1989).
[89] A. de Keizer, T. Michalski, and G. H. Findenegg, Pure Appl. Chem. **63**, 1495 (1991).
[90] W. D. Machin, Langmuir **10**, 1235 (1994).
[91] A. P. Y. Wong and M. H. W. Chan, Phys. Rev. Lett. **65**, 2567 (1990).
[92] A. P. Y. Wong, S. B. Kim, W. I. Goldburg, and M. H. W. Chan, Phys. Rev. Lett. **70**, 954 (1993).
[93] M. E. Fisher and H. Nakanishi, J. Chem. Phys. **75**, 5857 (1981).
[94] E. Bruno, U. Marini Bettolo Marconi, and R. Evans, Physica A **141**, 187 (1987).
[95] W. Kauzmann, Adv. Protein Chem. **14**, 1 (1959).
[96] C. Tanford, *The Hydrophobic Effect: Formation of Micelles and Biological Membranes* (Wiley–Interscience, New York, 1973).
[97] A. Ben-Naim, *Hydrophobic Interactions* (Plenum, New York, 1980).
[98] K. A. Dill, Biochemistry **29**, 7133 (1990).
[99] G. Hummer, S. Garde, A. E. Garcia, R. W. Impey, and M. Klein, J. Phys. Chem. B **102**, 10469 (1998).
[100] D. M. Huang and D. Chandler, Phys. Rev. E **61**, 1501 (2000).
[101] W. L. Jorgensen, J. Chandrasekhar, J. D. Madura, R. W. Impey, and M. Klein, J. Chem. Phys. **79**, 926 (1983).
[102] H. Tanaka, J. Chem. Phys. **105**, 5099 (1996).
[103] F. H. Stillinger and A. Rahman, J. Chem. Phys. **60**, 1545 (1974).
[104] F. Sciortino, P. H. Poole, U. Essmann, and H. E. Stanley, Phys. Rev. E **55**, 727 (1997).
[105] G. Stell, in *The Equilibrium Theory of Classical Fluids*, edited by H. L. Frisch and J. L. Lebowitz (Benjamin, New York, 1964), pp. II71–II226.
[106] J. K. Percus, in *The Equilibrium Theory of Classical Fluids*, edited by H. L. Frisch and J. L. Lebowitz (Benjamin, New York, 1964), pp. II30–II70.
[107] T. K. Vanderlick, L. E. Scriven, and H. T. Davis, J. Chem. Phys. **90**, 2422 (1989).
[108] J. K. Percus, J. Chem. Phys. **75**, 1316 (1981).
[109] J. K. Percus, J. Stat. Phys. **15**, 505 (1976).
[110] A. Robledo and C. Varea, J. Stat. Phys. **26**, 513 (1981).
[111] J. Fischer and U. Heinbuch, J. Chem. Phys. **88**, 1909 (1988).
[112] N. F. Carnahan and K. E. Starling, J. Chem. Phys. **51**, 635 (1969).
[113] T. K. Vanderlick, Ph.D. thesis, The University of Minnesota, 1988.